Basement domes in a greenschist facies context: Tectono-metamorphic evolution of the southern Quadrilátero Ferrífero, southeast Brazil

Renaud Caby, Mário da Costa Campos Neto

Basement domes in a greenschist facies context: Tectono-metamorphic evolution of the southern Quadrilátero Ferrífero, southeast Brazil

Renaud Caby[a], Mário da Costa Campos Neto[b]

[a] *Géosciences Montpellier, Université de Montpellier – CNRS, 2 Place E. Bataillon, 34090 Montpellier Cedex 5, France*

[b] *Universidade de São Paulo – USP, Instituto de Geociências, Cidade Universitária, CEP 05508-080 São Paulo, SP, Brazil*

Abstract

New petrostructural data are presented from the southeastern Quadrilátero Ferrífero, a distinct polyorogenic domain of the São Francisco Craton characterized by granite-gneiss domes and keel structures. The Minas Supergroup of Siderian age that hosts a huge volume of ferriferous sediments was deposited on the flat and eroded surface of the Archean basement. The domes of Archean gneisses and granites represent semi-rigid extrusions around which the Minas Supergroup accumulated in deep synclines with common triple junctions. This study focuses first on the petro-structural context of low-pressure thermal aureoles observed towards the dome margins. Pressure-temperature estimates on these mineral assemblages indicate nearly static burial to ≥ 10 km depths of the Minas Supergroup cover, followed by decompression and heating during the intrusion of pegmatites and granitoids of late Rhyacian age in basement and cover. The Archean basement and the thermal aureoles were severely overprinted by synkinematic greenschist facies metamorphism portrayed by chloritoid, chlorite, pyrophyllite, kyanite, phengitic mica and secondary biotite. This deep greenschist facies metamorphism (T ca. 420°C and P = 0.4 to 0.45 GPa) is regionally observed in all units from the domes and the keels ranging in age from Archean to Ediacaran. It is

concluded that this major tectono-metamorphic event relates to tectonic burial of the southern Quadrilatero Ferrifero below the west-verging nappes of the Araçuaí belt during the Early Paleozoic, as documented by 40Ar/39Ar ages of 490-485 Ma obtained on syn-kinematic metamorphic micas [Chauvet et al., 2001]. It is proposed that building up of the dome and keel tectonic style is first a consequence of the high-density contrast estimated around 0.5 g/cm$_3$ between the crystalline basement and the Minas Supergroup, the final architecture being achieved during the Cambro-Ordovician stage of the E-W Late Neoproterozoic collision.

Keywords: Quadrilátero Ferrífero; SE Brazil; Sagduction; Cambro-Ordovician tectonics; Polymetamorphism

1. Introduction

Nearly circular domes of granite-gneisses surrounded by keels of metasedimentary rocks and mafic metavolcanics represent the very common tectonic features of the Archean terrains (Chardon and Choukroune, 1996; Choukroune et al., 1995; Sandiford et al., 2004; Lin, 2005). Most crystalline domes are frequently fringed by the occurrences of high-temperature (HT) metamorphic rocks, whereas greenschist facies mineral assemblages are only present in the keels and schist belts far from the domes. There are many examples in Archean terrains of domes that clearly represent inliers of older basement rocks predating the deposition of sedimentary and volcanic units (the greenstones) preserved in the keels (Chardon and Choukroune 1996). In other Archean provinces there are many examples of domes entirely represented by more or less foliated magmatic rocks that intrude the greenstone keels (Parmenter et al., 2006 and references therein). Other examples show several superposed greenstone units and renewed magmatic events in the domes (François et al., 2014). Several

Phanerozoic domes or core complexes are genetically related with the diapiric emplacement of partially molten crust in active ocean-continent-plate margins (Rey et al., 2001; Teyssier and Whitney et al., 2002; Whitney et al., 2004, 2013).

In the eastern part of the São Francisco Craton (SFC), Minas Gerais, Brazil, the dome and keel structures of the Quadrilátero Ferrífero (QFe, Figures 1, 2) have been recognized and mapped in detail by Dorr (1969. This part of the SFC includes early Archean TTG-type granitoids and anatexites, Mesoarchean metasedimentary rocks of the Rio das Velhas Supergroup (RVS) and a younger Paleoproterozoic metasedimentary cover, the Minas Supergroup (MS) preserved out of the domes in several 30 to 150 km long synclines displaying an X-shape pattern and triple junctions (Figure 1) At variance with the common Archean situation such as reported from southern Africa, Australia and India, no mafic volcanics are present in the MS that instead includes several banded iron formations.

Several occurrences of HT metamorphic rocks have been described from small areas towards the periphery of the domes and half domes of the studied area (Marshak et al., 1992, 1997 and references therein). Several authors have proposed that this metamorphism represent "thermal aureoles" genetically related to the building up of the domes formed during the Paleoproterozoic (Alkmim and Marshak, 1998; Marshak et al., 1997). In contrast Hippert and Davis (2000) and Chauvet et al. (2001) have concluded that most structures observed in the MS relate to the Brasiliano orogeny of late Neoproterozoic to Early Paleozoic age that affected large domains of eastern Brazil. Recent age determinations by the U-Pb method suggest that the younger thermal event registered by some titanite, monazite and lesser zircon overgrowths around 2080-1940 Ma (Cutts et al., 2019; Dutra et al., 2019) is coeval with the dome and keel structures. However, the influence of an Early Paleozoic tectono-

78 metamorphic event is evidenced by Ar/Ar plateau ages of micas (Chauvet et al., 2001)
79 but also by local metamorphic overgrowths of zircon in the range of 580-520 Ma
80 (Aguilar et al., 2019). Understanding the structural history, the kinematics of the QFe
81 region and the building up of the domes and the keels of MS that hosts several world-
82 class iron mines from South America (Rosière et al., 2008) has major implications for
83 the reserves of this metal. This paper based on detailed field work and classical
84 petrostructural studies aims to clarify the structure, age and geodynamic evolution of
85 the dome and keel structures especially in the Bação dome area (Figure 3). How is it
86 possible to determine the regional metamorphic climax of tectonometamorphic
87 overprinting in a rigid basement of quartz-feldspathic rocks cut by nearly undeformed
88 granitoids ranging in age from the Archean to the Late Paleoproterozoic in this large
89 segment of Gondwana orogen ?
90 Common techniques of field mapping were utilized for this study and
91 supported by structural analyses at the outcrop and micro-scale. Criteria for identifying
92 structural overprinting were adopted on the basis of common deformation patterns
93 and/or similar mineral paragenesis. Our microstructural and petrological analyses were
94 aimed at defining the relationships between deformation and metamorphism. This
95 research is however hampered by the general poor exposures and severe weathering.
96
97 **2. Geological outline of the Quadrilatero Ferrífero**
98
99 *2.1. Archean-Paleoproterozoic rocks*
100 The QFe represents the southeastern part of the São Francisco Craton in Minas
101 Gerais-(Figures 1 & 2). The domes formed mainly by Paleoarchaean rocks encompass
102 gneisses, anatexites, granitoids among which abundant tonalite, trondjhemite and

103 granodiorite (TTG), metasedimentary rocks and greenstones including komatiites of
104 the Rio das Velhas Supergroup (RVS). A complex Archean evolution of the gneisses
105 of the Bação dome is constrained by the occurrence of amphibolitized dikes that cross-
106 cut the anatectic foliation (Cutts et al., 2019). In the Bação and the Bonfim domes
107 (Figure 2), layered and veined TTG orthogneisses of mainly granodioritic and tonalitic
108 composition commonly contain amphibolitic bands, whereas mafic stretched enclaves
109 are locally observed in gneissic granodiorite.
110 Two main units are classically distinguished in the RVS (Dorr, 1969). The
111 older Nova Lima Group consists of komatiites, basalts, phyllites, graphitic schists,
112 quartzites, banded iron formations, carbonates, amphibole and chlorite schists, while
113 the younger Maquiné Group includes metavolcanics, quartzites, schists and
114 conglomerates, younger andesites, dacites and volcaniclastic rocks.
115 Farina et al. (2015) and Moreira et al. (2016) distinguish several magmatic
116 events in the SFC: the Santa Bárbara Event (3.22 – 3.20 Ga), the RVS 1 event (2.93 –
117 2.85 Ga), the RVS 2 event (2.8-2.76 Ga) and the intrusion of K-rich granitoids during
118 the Mamona event (2.76 -2.68 Ga). The molasse-type sediments of the Maquiné
119 Group contain detrital zircon grains as young as 2730 Ma (Moreira et al., 2016). It is
120 worth noting that metasedimentary rocks of the Nova Lima and Maquiné Groups
121 exposed far from granitoids only underwent greenschist facies metamorphism at
122 distance ≥ 100 m from granitoid intrusions. A huge volume of leucocratic veins of
123 trondjhemitic affinity is observed in the Nova Lima Group coeval with felsic
124 volcanism and predating the emplacement of syn-to late kinematic 2.76 -2.68 Ga old
125 granites. This indicates that in several areas the Neoarchean deformation in the RVS
126 was minor and essentially connected with magma emplacement, anatexis having taken
127 place only close to large Archean igneous massifs. On the other hand, Machado et al.

(1992) obtained in the southern Bação dome U-Pb ages of monazite from pegmatites and of titanite from an amphibolite at 2060-2030 and 2059 ± 6 Ma, respectively, implying for these authors that the regional amphibolite facies metamorphism is of Paleoproterozoic age. Numerous U-Pb ages more recently obtained in the whole QFe on magmatic and metamorphic titanite, monazite and zircon (Aguilar et al., 2017; Cutts et al., 2019) are interpreted by these authors to be connected with thermal reheating emanating from the rising deep Archean crust. In the adjacent Mineiro Belt (Figure 1) that docked along the southern edge of the QFe, repeated Paleoproterozoic magmatic events relate to a long-lived accretionnary regime in part synchronous with the deposition of the MS and resulting from a collage of arcs between 2.47 and 2 Ga (Teixeira et al., 2015; Barbosa et al., 2015 and references therein).

2.2. The Minas Supergroup

Metasedimentary rocks of the MS are preserved in tight synclinoria and also involved in west-verging allochtonous units in the eastern part of the QFe (Chemale et al., 1994; Chauvet et al., 2001). Our field observations around the domes show that the base of this cover most frequently corresponds to an undetached stratigraphic unconformity represented by the basal Moeda Quartzite onto Archean rocks (granitoids, gneisses and low-grade or HT metasediments of the RVS) as stated by pioneering works (Door, 1969; Herz, 1978).

The MS represents a ≥ 6000 m-thick sequence of continental to marine sediments deposited on the SE edge of the SFC after 2.65 Ga (Rosière et al., 2008; Koglin et al., 2014). In the studied area, the Moeda Quartzite (up to 1300 m) is a regular unit only containing ≥ 2.6 Ga old detrital zircon grains, overlain by shales of the Batatal Formation, conformably overlain by the Itabira Group (950 m) that

153 includes the Cauê banded iron Formation (up to several hundreds of m) and carbonates
154 of the Gandarela Formation. The overlying Piracicaba Group (1300 m) represents
155 turbidites (Dutra et al., 2019). On top, the ≥ 3000 thick Sabará Group, separated by an
156 erosional unconformity, represents a foreland basin filled by polygenetic
157 conglomeratic formations, and semi-pelites and greywackes (Reis et al., 2002;
158 Alkmim and Martins Neto, 2012; Dutra et al., 2019). The source materiel is derived
159 from the erosion of plutono-volcanic arc assemblages from the Mineiro Belt (Noce et
160 al., 2000; Teixeira et al., 2015; Ávila et al., 2010; Barbosa et al., 2015).
161 The deposition age of the Minas Supergroup has been for long time a matter of
162 debate. The youngest detrital zircon grains from the auriferous Moeda Formation are
163 as young as 2680 ± 20 to 2610 Ma (Martinez Dopico et al., 2017). The thick
164 parautochtonous unit of aluminous metaquartzites that forms the Caraça range was
165 traditionally considered as equivalent to the Moeda quartzite and representing the base
166 of the MS. However, the age of 2.2 Ga of the youngest detrital zircon grains (Machado
167 et al., 1996) precludes this correlation. A whole rock Pb-Pb isochron age of 2.42 Ga
168 was obtained by Babinski et al. (1995) on a weakly deformed limestone from the
169 Gandarela Formation and a Pb-Pb age of 2.1 Ga on dolomitic lenses from the
170 Piracicaba Group, both dates interpreted as depositional ages. Based on the youngest
171 U-Pb ages of detrital zircon grains, the date of 2.036 ± 25 Ma represents the maximum
172 age of deposition of the Sabará Group (Dutra et al., 2019).
173
174 *2.3. Basal unconformity of the Minas Supergroup*
175 Contacts between the Moeda Quartzite (MS) and the underlying units (Archean
176 TTG gneisses, RVS metasedimentary rocks and granitoids) is everywhere sharp and
177 was first interpreted as a deformed erosional unconformity (Dorr, 1969; Herz, 1978

178 and references therein), but was later considered as tectonic by several authors
179 (Marshak et al., 1997 and references therein). The units of the MS lie always in their
180 right way-up stratigraphic order and Moeda Quatzite up to 600 m thick rests above the
181 Archean rocks on both sides of the Moeda syncline all along the western flank of the
182 Bação dome but is absent on its southern edge. Three localities where the
183 unconformity is well exposed and not obliterated by tectono-metamorphic overprint
184 are described below. 1/ Near the Fonte dos Anjos (utm: 0621068 - 7764433) the
185 angular unconformity between the sedimentary trend of underlying black metapelites
186 of the RVS and the steeply dipping Moeda Quartzite is of the order of 45°, and both
187 units are crosscut by the same greenschist-facies slaty cleavage. 2/ Near the Funil
188 railroad station, the spectacular stratigraphic unconformity of the basal Moeda
189 quartzite above high-temperature metapelites described in section 3 can be observed
190 along the railroad tracks (Figure 4 A). The stratigraphic unconformity above
191 retrogressed HT metapelites is not delineated by any pebbly horizon and begins
192 directly by channelized sandy layers. 3/ The contact between the Moeda Quartzite and
193 the Archean Mamona granite along the western limb of Bonfim dome has been
194 interpreted as a normal ductile fault delineated by mylonites (Hippertt, 1998). The
195 quartzite displays gently east dipping sedimentary bedding (20-30°) cut by steeper S1
196 metamorphic slaty cleavage delineated by white mica and chlorite, S1 becoming
197 almost parallel to the fine scale bedding of interlayered shales. The excellent outcrop
198 conditions reveal that several steeply dipping shear zones indeed cut the granite (see
199 section 5.1), but the granite is directly overlain either by white quatzite, or
200 progressively grades upward over a width of some meters into a ca. 25 m thick band of
201 moderately sheared metaarenite. The feldspars in this band have been progressively
202 replaced by metamorphic white micas and Mg-chlorite pseudomorphs after magmatic

biotite, depicted through their abundant tiny Fe-Ti mineral inclusions. The metaarenite band includes two intercalated layers of green metashale. We conclude that these mica-rich layers result from a strong chemical/pedogenetic alteration of the granite into a saprolite/arenite prior to the onset of sandy sedimentation.

3. Late Paleoproterozoic and Neoproterozoic rocks

The Late Paleoproterozoic/Mesoproterozoic Espinhaço Supergroup corresponds to the evolution of two superimposed sequences deposited between 1.75 and 0.9 Ga (Alkmim and Martins-Neto, 2012 and references therein). A correlation between the Itacolomi sequence exposed south of the Bação dome, in which the youngest detrital zircon grains gave a Pb-Pb age of 2.06 Ga (Machado et al., 1996 a; Machado and Gautier, 1996), and the Early Espinhaço Supergroup is presently accepted. This is in line with the peraluminous character of most quartzites from both units (commonly ≥ 10% kyanite content, as well as thin layers containig kyanite as the main mineral), at variance with the Moeda Quartzite surrounding the domes that is mostly free of Al-silicates. Quartzites of the Itacolomi Group (up to 1800 m thick), in which overall oblique bedding and ripple marks are ubiquitous rest unconformably (10 to 20°), or are detached from the underlying MS. The unit comprises aluminous quartzites, quartz-schists, metaconglomerates and grey to black quartz-poor to quartz-free metapelites, all rocks being pyrophyllite- and/or kyanite-rich as a result of their primary Al_2O_3 enrichment (assumed bauxitic component). Metarhyolites are also part of this package east of Ouro Branco, as reported from the entire Espinhaço belt. The Tamanduá Group exposed east of Caeté dome is younger than 1207 ± 28 Ma, the age of the youngest detrital zircon grains (Dutra et al., 2017). Metacarbonates from the Eastern Bambuí Group also exposed east of the Caeté dome were deposited after 560

228 Ma, the U-Pb concordia UPb age of the youngest detrital zircon grains collected at its
229 base from the Sete Lagoas Formation after Uhlein et al. (2017).
230
231 **4. High-temperature metamorphic evolution of the QFe**
232 Regional HT metamorphism and anatexis affected the 3.2 to 2.8 protoliths of
233 the domes around 2.8-2.7 Ga prior to the intrusion of a large volume of late-kinematic
234 Archean granitoids. The occurrence of cpx-plag-qz-bearing leucosomes in biotite-free
235 amphibolites of tholeiitic affinity points to dehydration melting consistent with local
236 temperatures ≥ 800° C (Rushmer, 1991; Rapp and Watson, 1995). Such elevated
237 temperatures may have been reached during the emplacement of dioritic/tonalitic
238 magmas, as proposed by Machado et al. (1992, 1996), Teixeira et al. (1998) and Noce
239 et al. (1998). TTG rocks have yielded crystallization ages of ca. 2860 Ma with
240 metamorphic overprint ranging from 2670 to 2705 Ma (LA-ICP-MS and SHRIMP U-
241 Pb ages, Lana et al. 2013). Al-rich metapelites concordant with anatectic gneisses
242 from the Bação dome contain the mineral assemblage cordierite-sillimanite-garnet ±
243 rutile. Pyrope contents ranging from 22 to 35 mole % (Gomes and Muller, 1987) point
244 to Archean metamorphic conditions near granulite facies. However, Paleoproterozoic
245 ages of metamorphic monazite and rutile bracketed between 2.1-2.0 Ga indicate that
246 HT metamorphic events considered as "thermal aureoles" also affected some domains
247 of the Archean basement. Moreover, since mid-temperature kyanite-chloritoid
248 assemblages are observed in the post-Espinhaço sequences that are younger than 1.75
249 Ga, it can be concluded that at least three successive metamorphic events can be
250 distinguished in the southern QFe, as suggested by Herz (1978), who presented the
251 first synthetic study of metamorphic facies from the QFe. The study of thermal

aureoles localized close to the dome margins is key to understanding the tectono-metamorphic evolution of the domes.

4.1. Geological context and pressure-temperature estimates for the thermal aureoles

Several 2760–2680 Ma potassic granites and granodiorites (Romano et al., 2013) such as the Mamona granite are devoid of thermal aureoles as they intrude high-temperature TTG-type gneisses, anatexites and amphibolites. Partial melting of mafic rocks (P = 0.5 GPa, T = 700 °C) has been dated by LA-ICP-MS at 2728 ± 4 Ma in the Bação dome (Farina et al., 2015). Archean granodiorite to tonalite plutons intruding the low-grade RVS commonly display igneous layering, show the classical features of magma mixing/mingling and are associated with several generations of aplite and granite veins.

4.1.1. Common low-pressure hornfelses

The Rio das Pedras two mica granitic pluton and other granodiorites of assumed Archean age cut at high angle the sedimentary bedding of thinly layered metapelites of the RVS. The inner aureole that is observed a few cm from magmatic contacts only consists in coarse-grained, non-anatectic two-mica hornfelses containing andalusite and cordierite in part replaced by white mica and pinite, respectively. Unaltered euhedral andalusite is locally preserved in metapelite showing preserved bedding (Figure 4 B). Such garnet-free mineral assemblage points to low-pressure conditions ≤ 3 kbar (Xu et al., 1994). The thermal aureole of the Serra Serinhas pluton has been severely overprinted, but is characterized by bent and brocken kyanite prisms up to several cm long only preserved in the core of meter-scale grey quartz boudins, whereas almost totally replaced by white micas is preserved in adjacent aluminous

277 quartzite. Graphitic metapelites from the inner aureole of the General Carneiro granite
278 stock contain prismatic sillimanite, staurolite and a strong tourmaline enrichment. The
279 Egenheiro Correia thermal aureole is related to the syn-kinematic emplacement of
280 granodiorite veins cutting steeply dipping anatectic metapelites (Figures 4 C, D).
281 Spectacular unoriented crystallization euhedral andalusite several cm across is
282 observed within a few decimeters from granitoid veins with diffuse margins (Figures 4
283 E, F).
284
285 *4.1.2. The Ibirité thermal aureole*
286 To the southwest of Belo Horizonte high-temperature metamorphism affected the
287 Sabará Group, separated by a major tectonic contact (the Serra do Curral Fault) from
288 the Belo Horizonte Archean complex of granitoids, anatexites and Al-rich schists of
289 the RVS (Romano, 1989). This thermal aureole close to town of Ibirité town was first
290 described by Romano (1989), Jordt-Evangelista et al. (1992) and Marshak et al.
291 (1992). Recently exposed outcrops show that these metamorphic rocks are related to
292 the emplacement of a few stocks of muscovite-rich granite and associated pegmatites,
293 both affected by solid-state vertical shearing synchronous with extensive greenschist
294 facies overprint. The ≥ 200 m wide spotted slates of the outer aureole to the south are
295 conspicuous for the occurrence of non-oriented brown biotite flakes commonly several
296 mm across that grew across the bedding planes of greywackes and chlorite-magnetite
297 semi-pelites (Figures 5A, B). The fine-scale bedding delineated by the Fe-rich layers is
298 fossilized in garnet and staurolite, with no microscopic evidence for a previous
299 cleavage. Metapelites mainly encompass undeformed primary mineral assemblages of
300 hornfelses more or less affected by syn-kinematic greenschist facies overprint as
301 described in section 5.2. Typical pelitic hornfelses with a random fabric collected a

few decimeters from a undeformed granodiorite stock contain unaltered andalusite pods and cordierite (Figure 5 C). Other two-mica rich samples contain biotite, andalusite and staurolite porphyroblasts. Kyanite is included in staurolite, whereas both minerals are included in poikilitic andalusite and cordierite. However, staurolite is squeletal almost retrogressed in mica-rich samples (Figure 5 D). In a few samples from the more massive layers, biotite shows negligible signs of destabilization (Figures 5 E, F) but its pseudomorphic syn-kinematic replacement by chlorite affected most samples (Figures 5 G, H). Sample BR925, a non-retrogressed metapelite, contains biotite (XMg = 0. 58-60; TiO_2 = 1.7%), minute garnet (≤ 200 μm) with composition alm 68 pyr 13 gro 6 spe 13, relict kyanite occasionally rimmed by fibrolite and/or included in cordierite (XMg = 0.76), staurolite (XFe = 0.75- 0.80), rare unaltered andalusite, unaltered plagioclase An 33-36 and magnetite. Minor fibrolite occurs at grain boundaries. The high Mn content of garnet and the K_20 loss of analysed biotites preclude calculating precise P/T conditions but a pressure of ≤ 4.5 kbar is deduced from the coexistence of the three Al -silicates for a temperature around ≤ 600° C. The only cleavage observed, that was later crenulated, is defined by tiny chlorite or white mica that clearly postdate the growths of the coarse-grained silicates that exhibit all stages of syn-kinematic greenschist facies retrogression as described in § 5.2. In agreement with Herz (1978), we consider that the development of this thermal aureole is unrelated to the dome, at variance with the interpretation of Jordt-Evangelista et al. (1992), Marshak et al. (1992), Hippertt and Davis (2000) and Brueckner et al. (2000).

4.1.3. The syn-kinematic Funil aureole

This occurrence of metamorphic RVS is adjacent to a foliated granodiorite of unknown age exposed 300 m west of the railroad station, in which syn-magmatic decameter-scale recumbent horizontal flow folds are observed. Slightly anatectic aluminous metapelites exposed 50 m above the Funil railroad station were studied in detail. The less retrogressed coarse-grained (≥ 0.5 cm) metapelite samples only preserved in decameter-sized boudins display the primary mineral assemblage garnet (pyr 20 to 24 mol%), prismatic sillimanite, altered andalusite, cordierite, Ti-rich biotite, staurolite, oligoclase and quartz (Figures 5 I, J). However most silicates suffered severe low-temperature recrystalization (Figures 5 K and L). Rutile, graphite, ilmenite and monazite are the accessory minerals. Undeformed pegmatite dikes cut the foliation. Mineral compositions of a weakly retrogressed sample using the TWEEQU software allow a rough estimate of metamorphic conditions of P = 6 kbar and T = 650° C. In contrast to the Ibirité aureole, this paragenesis is syn-kinematic as shown by relicts of a helicitic metamorphic cleavage preserved in garnet cores and delineated by quartz and ilmenite, and isoclinal folds sealed by polygonal arcs of brown biotite. The primary mineral assemblage described above could be possibly of Archean age. In an attempt to constrain the age of metamorphism, a non retrogressed biotite was analysed by the $^{39}Ar/^{40}Ar$ method and has provided two plateau ages bracketed of 3800 and 4000 Ma; these meaningless ages indicate the presence of excess ar. However, monazite from two pegmatites collected from this outcrop have given $^{207}Pb/^{206}Pb$ ages of 2030 and 2022 Ma (Machado et al., 1992).

5. Low-temperature greenschist facies metamorphic overprint

Our sampling supports that synkinematic greenschist facies metamorphic overprint affected all rocks of the QFe. This retrograde metamorphic event is discrete in Archean gneisses, granitoids, mafic rocks and paragneisses from the RVS, but prograde in metasedimentary rocks from the Bambuí Group, Espinhaço, Minas Supergroups and from the RVS exposed far from the thermal aureoles described in section 4.

5.1. Gneisses and granitoids

The microscopic observation of about 30 samples of granitoids and gneisses from different areas of the Bação dome and the eastern Bonfim dome has revealed the ubiquitous overprint of greenschist facies mineral assemblages. In gneisses located close to the eastern margin of the Bonfim Dome, the high amount of secondary epidote formed as a result of the breakdown of the former plagioclase that is entirely recrystallized into albite. Most of the primary brown biotite of such Archean gneisses has recrystallized into minute sub-grains of secondary Ti-poor pale brown biotite. Associated pendants of mafic metasedimentary rocks and metaintrusives contain the syn-kinematic assemblage Mg-rich biotite to phlogopite, Mg chlorite, tremolite and porphyroblastic albite. The Archean granitoids exposed to the SW of Brumadinho display in hand specimen random fabric as the cross-cutting granite dikes dated at 2703 Ma (Machado and Carneiro, 1992). However, microscopic investigations reveal that the granite dikes and the country gneisses are cut by the same incipient vertical cataclastic cleavage delineated by ductilely deformed quartz, minute white mica and pale Ti-poor biotite (Figure 6 A and B), the shape fabric of which delineates syn-metamorphic slickensides. Primary muscovite from associated pegmatites, in contrast,

375 is simply kinked and microfolded. Granodiorite exposed around Itabirito is affected by
376 brittle deformation in the form of a system of low-angle microfractures cutting the
377 nearly isotropic igneous structure, with minor amounts of preserved K-feldspar mostly
378 replaced by white mica. The numerous microfissures, generally 1 to 2 mm wide, are
379 filled by phengitic mica in equilibrium with pale brown biotite, epidote, albite and
380 calcite (Figure 6 C).

381 The slightly deformed 2.7 Ga Mamona granite (Figure 2) is cut by several cm-
382 thick steep N-S normal faults and mylonitic bands. Large parts of the granite,
383 however, show in thin section a cataclastic microstructure but also thin protomylonite
384 bands (Figure 6 D). Bluish quartz grains display a progressive mosaic recrystalization.
385 Titaniferous magmatic biotite that has exsolved abundant Fe-Ti granules has been
386 almost completely replaced by polycrystalline aggregates of green Fe-rich and Ti-poor
387 biotite, that is also concentrated in fractures cutting the perthitic K-feldspar megacrysts
388 and surrounded by minute sub-grains of fresh microcline (Figure 6 E). Other
389 undeformed coarse-grained domains of the granite are also cut by a dense system of
390 veinlets, some filled by secondary white mica, olive green to pale-brown biotite, and
391 Mg-chlorite, others by epidote. In some protomylonite bands, the perthitic K-feldspar
392 clasts are almost recrystallized into fresh microcline and white mica set up in a quartz-
393 albite-biotite schistose matrix (Figure 6 F). The ultramylonite bands (2-5 mm wide)
394 made of alternating dark green biotite, and quartzo-albitic bands, while others contain
395 white mica aggregates as the chief mineral (Figure 6 H). The same mineral
396 assemblage is observed in the unconformable Moeda quartzite (Figure 6I). White
397 micas are Fe-rich phengites (4% FeO) with Si = 3.22 to 3.25, in equilibrium with Ti-
398 poor biotite ($\leq$ 1.4 TiO_2 weight%, XMg = 0.62), albite and secondary microcline, thus
399 allowing to use Massonne's phengite geobarometer (Massonne and Schreyer, 1987).

Pressure conditions are thus estimated at 4.5 kbar, T around 420°C being constrained by the coexistence of biotite and microcline and by the regional occurrence of kyanite and pyrophyllite.

In most felsic gneisses such as around Itabirito, São Gonçalo de Bação and the Amaratima anatectic granodioritic to trondjhemitic orthogneisses, undeformed secondary white mica and biotite of larger size than in the Mamona granite (mean grain size = 1 mm) are observed either with a random fabric, or displaying a shape fabric parallel to steep striations on reverse east-dipping ductile fault zones. Some of the granodiorite gneisses with preserved high-temperature fabric in hand specimen and displaying abundant restitic bands underwent complete static recrystallization. The second mineral assemblage epidote, albite, biotite, white mica and carbonate totally erased the former high-temperature mineralogy and fabric. Close to the reverse shear bands dipping 30° to the SE as the down-dip stretching lineation the microstructure is porpyroclastic with mosaic quartz-albite and a high amount of minute white mica formed through progressive breakdown of the K-feldspar in the center of the shear band, the core of which is highly enriched in phengitic mica. Retrogressed amphibolites and tonalitic gneisses are observed along the border zones of massive metaintrusives. These rocks frequently display greenschist facies protomylonitic fabrics (actinolite, Mg-chlorite, green biotite, epidote and albite) mostly corresponding to the reactivation of the former high-temperature foliation, but coarse-grained garnet amphibolites contain well-preserved pargasitic brown amphibole only fringed by a $\leq$ 20 μm thick actinolite rim. In other samples the calcic plagioclase is totally recrystallized to epidote and albite with myrmekitic clinozoisite reaction rims between plagioclase and amphibole.

425 *5. 2. Greenschist facies overprint of the thermal aureoles*

426

427 Classical retrograde mineral reactions are observed in most metapelitic
428 hornfelses from several localities. In the Ibirité hornfelses, the primary biotite shows
429 all stages of partial to complete replacement by chlorite (XMg = 0. 65), (Figures 5 G,
430 H). In sheared metapelites, the white mica that defines the foliation formed in part
431 through the replacement of andalusite poikiloblasts and has been determined as Fe-
432 muscovite containing 7 to 10% paragonite. The foliation of Fe-Mg schists is defined
433 by syn-kinematic chlorite, the Mn-rich almandine being considered as low-
434 temperature syn-kinematic porphyroblasts. In most metapelites cordierite is replaced
435 by pinite. In other samples, squeletal grains of relict staurolite (Figure 5 D) are
436 enriched in zinc (up to 4% ZnO), a chemical feature interpreted as the result of
437 staurolite re-equilibration, thus evidencing that the minute oriented paragonitic
438 muscovite in microtextural equilibrium with albite formed during the second
439 metamorphic episode. Euhedral andalusite prisms from the Engenheiro Coreia aureole
440 are entirely replaced by a groundmass of pyrophylite, cordierite by pinite, the pyrope-
441 rich garnet relicts being hardly preserved in cm-scale Mg-chlorite pseudomorphs. In
442 retrogressed anatectic metapelites from the Funil station, relict prismatic sillimanite is
443 partly replaced by aggregates of white mica (Figures 5 I, J) and the pyrope-rich garnet
444 almost entirely replaced by Mg-chlorite. Rosettes of chloritoid crystalized in the site,
445 or as reaction rim around relict staurolite (Figures 5 K-L). Phlogopite, Mg-chlorite,
446 secondary white mica and albite represent the syn-kinematic matrix mineral
447 assemblage with diversely oriented relicts of primary biotite.

448

449 *5. 3. Greenschist facies mineral assemblages of common metapelites*

450 Far from the thermal aureoles most RVS metasedimentary rocks are affected
451 by the same greenschist facies slaty cleavage (Figure 6 I) than rocks of the
452 unconformable Minas and Espinhaço Supergroups. It is thus not possible to decipher
453 under the microscope if an Archean greenschist facies mineralogy and cleavage were
454 already present or not in the RVS, in agreement with the interrogations of Herz (1978).
455 Metapelites and quartz schists are characterized by the ubiquitous syn-kinematic
456 crystallization of white micas -among which pyrophyllite in Al-rich pelites- whereas
457 chlorite and Fe-chloritoid are observed in Fe-Mg rich compositions (Dorr, 1969;
458 Schorscher et al., 1982; Herz, 1978). The widespread occurrence of kyanite ±
459 pyrophyllite is observed in aluminous shales and quartzites from both the Itacolomi
460 group, the MS (Piracicaba Group) and the RVS. Around Ouro Preto, the
461 crystallization of kyanite took place towards the end of the development of the slaty
462 cleavage defined by white micas and hematite that cuts at rather low angles the
463 perfectly preserved millimeter-thick sedimentary bedding (Figure 7A). Kyanite
464 commonly crystallized as unstrained rosettes in the S1, associated with quartz pods
465 containing blue kyanite prisms up to several cm long. Though some pyrophyllite-
466 bearing cracks occasionally overprint the kyanite crystals, most samples show a
467 microstructural equilibrium between pyrophyllite and kyanite, thus suggesting
468 regional temperature around 420°C, the admitted temperature for the inversion
469 pyrophyllite/kyanite at 4-5 kbar. The analyzed white mica from a kyanite metapelite
470 from the Itacolomi peak is a Fe-muscovite, but in metaporphyries from the Ouro
471 Branco ridge, the white mica is a phengite (Si 3.15- 3.23), thus again constraining a
472 pressure around 4.5 kbar. In the Moeda syncline, the S1 cleavage in Fe-rich layers
473 from the Cauê Formation defined by the planar fabric of hematite commonly makes an

474 angle of a few degrees to the ubiquitous millimeter-scale rhythmic sedimentary
475 bedding. Needles of Fe-rich amphibole of the grunerite series, actinolite, tremolite and
476 talc are observed in Ca-Mg-Fe-layers and these minerals also form polygonal arcs of
477 microfolds. Mineral assemblages from impure carbonates of the Bambuí Group
478 exposed northeast of the Caeté dome are also of deep greenschist facies grade and
479 coeval with recumbent folds, as observed in centimeter-thick layers derived from
480 marly shale that contains Mg-chlorite, white mica, talc, epidote, tremolite, albite and
481 acicular rutile.
482
483 *5. 4. Pressure and temperature field gradient in the eastern edge of the Bação Dome*
484 East of Mariana garnet-staurolite assemblages exposed near Ribeirão do Carmo show
485 a fossilized low-temperature prograde stage evidenced by chloritoid inclusions in
486 garnet cores (Figures 7 B, C), whereas staurolite crystalized in the chlorite-biotite
487 matrix. This prograde mineral suite is thus the opposite with that observed in the
488 thermal aureoles. Chauvet et al. (2001) studied in detail metapelite samples from the
489 Passagem de Mariana gold mine. These authors report the mineral assemblage
490 kyanite-garnet-staurolite-biotite-white mica-phlogopite-carbonate-quartz, for which
491 they calculated metamorphic pressures of P = 6.8 to 9.8 kbar and temperatures from
492 470 to 520°C. Biotite and white mica from these rocks have given laser spot fusion
493 Ar/Ar ages of 485-490 Ma (Chauvet et al., 2001).
494
495 **6. Architecture and kinematics**
496
497 *6.1. Major structures*

The sinuous geometry of synclines of the MS shares several characteristics of classical "Dome and keel" structures. Significant are the triple point 3D intersections of synclines such as on both extremities of the Moeda syncline that are characteristic of sagduction tectonics (Choukroune et al., 1995; Chardon and Choukroune, 1996). In the east the RVS is part of the low-angle Gandarela-Caraça allochthon in which the overall E-W elongation of pebbles from the Maquiné Group indicates a regular direction of transport to the WNW.

South of Belo Horizonte, the SW-NE regular belt of MS can be continuously followed from the Serra do Curral to Sabará. The MS is delimited from the Belo Horizonte Archean granite-gneiss complex by a major SE-dipping contact first interpreted as a thrust by Romano (1989) and along which the whole group lies upside down, as confirmed by Sanglard et al. (2014). However, shear criteria (S/C planes) reported by Hippertt and Davis (2000) indicate a normal movement along this contact delineated by phyllonites that may post-dates the thrusting and the stratigraphic inversion.

The geometry of the Bação granite-gneiss complex has been interpreted as an asymmetric west-verging dome (Chauvet et al. 2001). All along the western margin of the dome, the unconformable MS is steeply dipping or locally upside-down. Around Ouro Preto, the main thrust zone becomes nearly flat and is delineated by reverse metamorphism portrayed in metapelites by the biotite and staurolite-in isograds (Chauvet et al., 2001). The Dom Bosco synform reworks a system of west-directed imbricates and nappes involving the RVS and the Itacolomi sequence. Refolded isoclinal folds affecting carbonates of the Bambuí Supergroup are observed east of the Caeté Complex (Figure 7 J).

6. 2. Structural style, fold geometry and strain markers in the Minas Supergroup around the Bação dome

The MS was involved in major first-order tight synclines (the Moeda, the Vargem do Lima and the Gandarela synclines) that can be traced over several tens of km, the original and regular lithology being perfectly preserved. However, the apparent thickness of the lower MS (without the Sabará Group) is locally reduced to less than 2000 m, for example across the middle part of the Moeda syncline, thus suggesting ≥ 300% of thinning of the whole MS. The lack of associated anticlines around the domes is significant. The high dips of bedding planes, commonly 60 to 85° in fold limbs, and the steep bedding/cleavage intersections suggest the existence of steeply plunging folds, as observed along the western limb of the Moeda syncline; small-scale parasitic folds are observed. One single slaty cleavage (S1) clearly cuts the bedding of the Moeda Quartzite with high angle refraction but S1 in associated chlorite schist layers becomes almost parallel to bedding indicates severe layering-parallel nearly vertical extension shown by steeply dipping stretching lineations. The 3D outcrops along the Chafariz ridge, ca. 6 km west of Ouro Preto (Figure 7 D), allow observing in the Cauê Formation, meter to decameter-sized curviplanar folds and hectometer-sized lenses with associated steeply-dipping tongue-like hinges, overprinted by post-S1 down-facing folds with horizontal axial planes. The steeply dipping cleavage (S1) observed in planar domains mostly intersects the bedding planes at rather low angle (≤ 5 to 10°), the intersection of both surfaces corresponding to the white mica and hematite shape fabrics and bearing pronounced steeply-dipping stretching L1 lineations delineated by the elongate shape of minute quartz grains. Kyanite and amphibole needles in rocks of appropriate bulk compositions crystallized parallel to the steeply plunging S0/S1 intersections. Planar domains also comprise

548 bedding-parallel slides or cryptic shear zones (Hippertt and Davis, 2000) that delimit
549 symmetric and asymmetric lenses, suggestive of severe thinning of the Fe formations.
550 Mylonites *s.s.* and phyllonites could not be identified, since metasedimentary rocks of
551 chemical origin are predominant. In some pelitic carbone-rich layers the lack of clast
552 asymmetry observed in X-Z thin sections reveals domains that were subjected to
553 nearly coaxial deformation (Figure 7 E). The Fe layers also include chaotic folded
554 domains (Figure 7 F), in which disharmonic folds, rootless folds and low-angle slides
555 that delimit tectonic lenses are observed, whereas numerous sub-perpendicular quartz
556 tension gashes occur in more competent layers. Subsidiary post S1 upright P2 folds as
557 well as younger sets of conjugate box folds are also observed. Such complex apparent
558 polyphase structures are interpreted as the result of progressive deformation and
559 bedding parallel individual sinking of the dense Fe-rich layers of the Cauê Formation
560 that contains iron-rich layers with densities bracketed between 3.4 and 4.8, as argued
561 by Hippertt and Davis (2000). Significant are the two triple junctions at both
562 terminations of the Moeda syncline, features that preclude homogeneous direction of
563 horizontal shortening and thus suggestive of sagduction according to Choukroune et
564 al. (1995).
565
566 *6.3. Estimates of bulk vertical elongation*
567 The deformation registered in the Archean gneisses is difficult to estimate
568 owing to the frequent reactivation of the steeply dipping gneissic foliation by discrete
569 low-temperature shearing. Importantly, the trajectories of the reactivated foliation tend
570 to parallel the Bação dome margins, especially along its western and southern limits,
571 but these depart from the mean steep NNW trend of the Archean HT foliations. A
572 great number (≤1% volume) of millimeter thick nearly horizontal fractures sealed by

phengitic mica are observed in leucogranites around Itabirito. In a cross-cutting mafic dike exposed north of this town, the measured frequency of sub-horizontal dilation fractures a few mm wide filled by actinolite, Mg-biotite and chlorite indicates a nearly vertical elongation of about 5% (Figure 7 H).

The distribution of S-C fabrics and XZ finite strain ellipses across the Moeda syncline (Hippertt and Davis, 2000) indicates higher values (RXZ up to 7.6 approaching the dome contacts compared to 2.2 in the core of the syncline). The amount of vertical elongation has been estimated from the geometry of quartz boudins and tension gashes from schists of the Batatais Formation east of the Bonfim dome at Belo Vale pass. The steeply dipping syn-kinematic internal fabric of fibrous quartz (L1) is delineated by a dense network of Fe amphibole and epidote fibers several cm to tens of cm long. The X-Z section is suggestive of 200% vertical elongation and the 3D geometry of quartz pods indicates severe flattening. At this locality the black metapelites of the Batatais Formation have thus the characters of a ca. 30 m thick shear band for which, the shear sense indicators from the sigmoidal quartz boudins evidence a reverse syn-metamorphic movement. Curiously, opposite shear senses are also observed laterally in this band. In ferruginous layers of the upper part of the Cauê Formation, the "chocolate tablet" crack-seal fabric of some rigid ferruginous dolomitic layers evidences about 30% of vertical elongation measured parallel to quartz fibers (X) associated to ca. 10% of oblique elongation (Figure 7 G). The hinges of microfolds from ductilely deformed Fe-carbonate layers are commonly sealed by the crystallization of undeformed needles and polygonal arcs of Fe-amphibole. The vertical spaced S1 cleavage cutting at rather low angles the bedding planes of such impure carbonates displays the characters of millimeter-scale shears, the observed displacements suggesting about 30% of vertical elongation in fold limbs, but nearly

598 pure flatening as well as shear in opposite direction are also observed in the most
599 ductile layers. The less deformed rocks, in contrast, such as the Gandarela dolomite
600 layers from the horizontal hinge of the large Gandarela syncline, display an upright
601 spaced dissolution cleavage and associated microfolds consistent with about 20% of
602 nearly NW-SE horizontal shortening. These rough estimates and the rather high
603 ductility of most lithologies suggest that the large MS synclines are non-parallel and
604 share the characters of tongue-like folds in limbs indicative of strong nearly vertical
605 elongation.
606
607 *6. 4. Evidence for tectonic unroofing SE of the Bação Dome*
608 The earliest syn-metamorphic deformation hardly observed in the
609 unconformable Moeda quartzite close to the Funil station is a west-dipping penetrative
610 cleavage (S1) delineated by minute white mica that is axial plane of minor N-S
611 asymmetric folds, but in overlying black schists S1 is a slaty cleavage that is passively
612 deformed by asymmetric east-verging folds displaying axial planar crenulation
613 cleavage (S2). In underlying metapelites from the basement described in section 5.2.,
614 the HT foliation has been progressively reworked over a thickness of about 100 meters
615 below the quartzite, with complete low-temperature break down of sillimanite and
616 garnet. The strongly developed cleavage in the Cauê hematitites is related to sliding
617 nearly parallel to bedding, as evidenced by the frequent crystallization of penetrative
618 quartz + hematite fibers along bedding planes. In the overlying carbonates exposed in
619 the Fecho do Funil quarry, the dolomite layers have suffered a spectacular horizontal
620 boudinage accompanied by disharmonic isoclinal folds (Figures 7 I). The oldest
621 deformation in these rocks is a SE-dipping pencil lineation (L1) well defined in micro-
622 conglomeratic layers that display the mineral assemblage calcite-phlogopite-talc-

623 epidote-quartz ± hematite. Thus, the Fecho do Funil section clearly evidences E to
624 ESE -verging ductile shear and low-angle normal sliding that resulted in a significant
625 thinning (≥ 30%) of the lithostratigraphic pile (Figure 8).
626
627 **7. Discussion**
628
629 *7. 1. Archean and Paleoproterozoic evolution*
630
631 Zircon ages of the gneisses record two age groups of 2925-2900 Ma and 2795
632 Ma (Lana et al., 2013; Romano et al., 2013; Farina et al., 2015), but also well defined
633 2775 Ma zircon rims (Cutts et al., 2019). 2700 Ma old granitic veins and leucosomes
634 were intruded synchronously with late- to post-kinematic K-rich granites during the
635 Mamona event. The steep NW-SE foliations and the steeply dipping mineral lineations
636 in the Bação dome are consistent with HT vertical flow and coeval magmatism, as
637 reported worldwide in gneiss domes (Teyssier and Whitney, 2002; Whitney et al.,
638 2004; François et al., 2014 and references therein). It is thus concluded that incipient
639 Archean stage of vertical exhumation and doming of the gneissic-anatectic crust took
640 place with the characters of buoyancy-driven flow coeval with incipient sagduction of
641 the RVS. North of the Bação dome, sedimentary rocks of the RVS were involved in
642 open folds with a NW-SE tectonic grain, some domains lacking a slaty cleavage. This
643 suggests that such domains represent high-crustal levels of the Archean crust that
644 escaped ductile deformation but instead were affected by nearly static low-temperature
645 recrystallization. The surprising fair preservation of sedimentary features in shales and
646 spinifex structures in komatiites is a charater of greenstone and hornefelse.

After its cooling and stabilization around 2.6 Ga, the Archean crust underwent several km of erosion and was unconformably overlain by the shallow water sediments of the MS deposited between ca. 2450 and 2036 ± 25 Ma (Dutra et al., 2019). Since synform relics of MS are preserved in the central part of the SFC (Figure 1), it is assumed that the QFe was entirely buried under the MS cover. Rhyacian reheating of the crystalline crust is demonstrated by U-Pb ages of titanite and monazite from the Archean gneisses and granitoids bracketted between 2100 and 1940 Ma (Machado et al., 1992; Noce et al., 1998; Farina et al., 2015; Cutts et al., 2019). Rhyacian migmatization of 2.7 Ga protoliths has been recently uncovered ca. 75 km west of the Bação dome by large zircon rims dated at 2048-2034 Ma (Carvalho et al., 2017). Except the Funil aureole that is synkinematic and linked with the emplacement of a granitoid sheet of assumed Rhyacian age, the other studied thermal aureoles display random fabrics of common low-pressure hornfelses. Metamorphic monazite from the Sabará Group in the same area has been dated at 2034 ± 11 Ma (Sanglard et al., 2013). This very precise metamorphic age is thus in the range of the deposition age of the Sabará Group itself (2036 ± 25 Ma after Dutra et al., 2019). Such coincidence strongly suggests that heat advection with sharp thermal gradients took place under an extensional setting coeval with limited magma emplacement and synchronous with deposition of the Sabará Group.

Based on geochemical and isotopic data, several authors suggest a back-arc environment during this Late Paleoproterozoic period (Aguilar et al., 2017 and references therein). For these authors, metamorphism of Rhyacian age is regarded as a syn-collisional event followed by slow cooling until 1930 Ma, but such interpretation is not supported by kinematic data. Eclogites of assumed Paleoproterozoic age (P = 18.5 kbar, T = 626 °C) have been recently discovered in the northwestern part of the

672 Bação dome (Chaves et al., 2019), but the context of this occurrence is not precised.
673 Further field and geochronological data are required to propose a more complex
674 evolution, as depicted elsewhere. For example, a long-lived magmatic evolution of
675 150 Ma is evidenced in west Africa in the Paleoproterozoic Baoulé-Mossi Domain
676 (West African craton) that was subjected to continuous magmatic activity during
677 accretionary process and collage of arc systems, with the existence of a magmatic
678 front migrating westward at a rate of 35 km /Ma (Parra-Avila et al., 2017). Such
679 Paleoproterozoic evolution is however at much variance with Phanerozoic arc
680 evolutions, as portrayed for example by the Tyrhenian arc (central Italy) in which the
681 Elba Island granitoid was emplaced in an extensional setting at 5.9 Ma and ca. 5 km
682 depths (Caggianelli et al., 2014).
683 From a geodynamic point of view, the Late Rhyacian thermo-tectonic event
684 recorded in both the Bação dome and the MS is thus considered as the thermal
685 reactivation of the Archean vertical structures below ca. 10 km of the MS cover and
686 does not relate to a collisional process. Then the area was in part covered by the
687 molassic sediments of the Espinhaço/ Itacolomi Group of assumed Statherian age, the
688 latter lying in slight unconformity above the upper MS. The area was also intruded by
689 anorogenic sub-alkaline gabbros dated at 1714 ± 5 Ma (Silva et al., 1995) and by three
690 generations of mafic dikes, the younger dated at 766 ± 36 Ma (all U-Pb ages on
691 baddelleyite, Cederberg, 2013). At variance with current interpretations, our
692 petrographic observations point that the Archean crust as well as the thermal aureoles
693 were subsequently affected by severe syn-kinematic greenschist facies metamorphic
694 overprint, as discussed below.
695
696 *7. 2. Low-temperature tectono-metamorphic overprint of the QFe*

The petrological data presented in this paper document an unraveled cryptic or significant deep greenschist facies metamorphic overprint in every kind of igneous and anatectic rock from the QFe that has been overlooked by previous authors. The ubiquitous retrograde metamorphism of granites and gneisses comprises white mica among which phengite, Ti-poor biotite, chlorite, albite, epidote, carbonates, hematite and sulphides. Mafic rocks also show retrograde minerals such as chlorite, green biotite, phlogopite, chloritoid, actinolite and blue-green amphiboles. The Paleoproterozoic thermal aureoles give classical examples of low-temperature metamorphic overprint among which chloritoid, Ti-poor biotite, white mica and Mg-chlorite that have replaced the high-temperature Al and Fe-Mg silicates previously equilibrated at $T \geq 550°$ C. Away from the thermal aureoles, the Archean metasedimentary rocks show the development of this greenschist facies metamorphic overprint, and the observed new incipient spaced metamorphic cleavage is parallel and coeval with that formed in the overlying monocyclic Minas and Itacolomi supergroup (identical orientation of structures, kinematics and mineralogy). Since the semi-brittle regime in crystalline rocks of the domes was synchronous with the greenschist facies cleavage observed in adjacent RVS and MS, we consider that the whole QFe was subjected to regional synkinematic metamorphism best portrayed in aluminous and peraluminous metasedimentary rocks by the crystallization of kyanite in equilibrium with pyrophyllite, implying regional temperature of about 420° C and pressure around 4.5 kbar in the whole QFe, thus consistent with tectonic burial of about 10 to 15 km (Figure 9). Significant higher T and P (T ca. 500° C, P around 8 kbar, Chauvet et al., 2001) are only reported east of the Bação dome, from the Ouro Preto-Mariana area towards the front of the west-verging nappes of the Araçuaí Belt.

722 The 3D geometry deduced from the dips of the unconformable MS all around
723 the domes would argue for a higher rate of exhumation of the basement. However,
724 similar metamorphic conditions of T about 420° C and ca. 4.5 kbar pressure are so far
725 recorded both in the domes and in the synclines of the MS and there is no petrological
726 evidence for progressive temperature increase for this metamorphic overprint towards
727 the center of the Bação dome, thus implying similar regional burial of ca. 10 to 12 km
728 under a cratonic-type geotherm of ca. 30° C/km. The intensity of low-temperature
729 retrograde reactions in gneisses and granitoids depends on the amount of shearing that
730 was assisted by fluid circulation. The greenschist facies regional metamorphic
731 overprint in the Bação crystalline complex was roughly coeval with doming/upward
732 extrusion as recorded by greenschist facies nearly horizontal crack-seal tension gashes
733 in dikes and steeply dipping stretching lineations in the crystalline rocks. Tectonic
734 unroofing at its southeastern edge is shown by the syn- to late-greenschist facies
735 kinematics recorded in the Fecho do Funil quarry. Unroofing of the southern extremity
736 of the Bação dome is shown by the syn- to late-greenschist facies kinematics recorded
737 in the Fecho do Funil quarry. This SE-verging ductile deformation relates to an
738 apparent single tectonic pulse and thus necessarily younger than the westward
739 emplacement of the overlying, now eroded, west-directed internal nappes. These
740 comprise Archean gneisses of the Santa Barbara complex but also inliers of the RVS,
741 MS and Itacolomi units, all affected by sillimanite grade metamorphism east of 43°
742 40'. The latter units are part of the reworked cratonic edge exposed in front of the
743 Araçuaí orogen.
744 The syn-metamorphic east-directed gravitational backsliding of the Ouro Preto-
745 Mariana nappes documented by Chauvet et al. (2001) is thus regarded as a
746 consequence of the basement exhumation of the Bação complex. Endo and Fonseca

747 (1992) and Almeida Abreu and Pflug (1994) consider that the MS and the overlying
748 Itacolomi Formation from the eastern part of the QFe were involved in westward
749 thrusting in the order of 30 km above a flat sole thrust. The amplitude of this thrusting
750 may exceed 45 km according to Marshak et al. (1989), but is on the order of 150 km
751 for Chemale et al. (1994).
752 In the northwesten part of the QFe, south of Belo Horizonte, the major
753 southeast dipping fault all along the Curral-Sabará belt (Romano, 1989) is tentatively
754 interpreted as the emergence of such major low-angle thrust connected with the
755 inverted polarity of the MS along the Serra do Curral-Sabará belt. According to this
756 author, this main thrusting event was followed by later uplift of the Belo Horizonte
757 complex that belongs to the less reactivated part of the SFC. It is thus concluded that
758 this NW-directed thrusting was coeval with the nearly vertical deformation observed
759 throughout the eastern QFe.
760
761 *7. 3. Kinematic constraints and comparisons with Phanerozoic low-temperature*
762 *basement domes and extrusions*
763
764 Doming and basement extrusions are common in many collisional mountain
765 ranges. In the Western Alps and the Pyrenees, the upward extrusion of the Hercynian
766 crust during the Tertiary contraction has been documented for a long time. Such mid-
767 crustal basement tectonics is in part inherited from differential subsidence of Mesozoic
768 basins accommodated by syn-sedimentary normal faults and basement highs. In the
769 QFe, no syn-sedimentary extensional faults have been recognized so far and the
770 uniformity of sedimentary facies of the MS suggests that the domes were entirely

771 covered by the MS (ca. 6 to 10 km), though a higher subsidence rate of the MS may
772 have taken place in areas rooted by the RVS and komatiites.
773 In the Western Alps, the reactivated Hercynian basement of the external
774 crystalline massifs was affected by steep ductile syn-metamorphic shear zones and
775 associated vertical shear (P = 5 ± 1 kbar, T = 400 ± 50 °C, ~~Rossi et al., 2005;~~ Rolland
776 et al., 2003; 2008). Vertical stretching is also observed in the tight Mesozoic synclines
777 (Gratier and Vialon, 1980), where chloritoid has been reported. For Dumont (1988),
778 this upward Alpine basement exhumation from mid crustal levels was nearly
779 synchronous with a major low angle blind thrust at depth. Refining this model,
780 Rolland et al. (2008) and Egli et al. (2017) concluded that final "pop up" extrusion of
781 the ca. 10 km wide and 35 km long Mont Blanc massif is ca. 20 Ma younger than the
782 horizontal westward emplacement of the higher nappes of more internal origin, but
783 coeval with the latest westward displacement of the whole Alpine Range.
784 The nearly circular structure of the Bação dome precludes important E-W
785 horizontal shortening. Only a few retrograde low-angle shear zones occur in the domes
786 compared to the strong ductile deformation in the MS synclines, in which horizontal
787 shortening was mainly accommodated by vertical elongation. Thus, the crystalline
788 rocks of the Bação dome behaved nearly rigidly but were affected by moderate
789 vertical elongation. In the north of the QFe, the Serra do Curral-Sabará belt and the
790 Gandarela nappe system, on the contrary show effects of global WNW-ESE
791 shortening with a top to the NW vergence.
792
793 *7. 4. Towards a geodynamic model of the QFe*
794

795 It is proposed that exhumation and cold extrusion of the Archaean basement (T
796 ≤ 420- 450° C) is first a direct consequence of an exceptionally strong buoyancy
797 contrast between the Archean gneisses and granitoids in one hand, and supracrustal
798 units that host abundant Fe layers. An assumed moderate density contrast of ≤ 0.1
799 between granitoids and the RVS is likely, taking into account the small volume of
800 greenstones mostly converted into chlorite-talc-serpentine assemblages. However the
801 MS hosts a huge volume of banded iron formations (ca. 500 to 1000 m according to
802 Dorr, 1963), with densities bracketed between 3.4 and 4.8 (Hippert and Davis, 2000).
803 Thus, an estimated high buoyancy contrast between the domes and the keels of the
804 order of 0.4 g. cm^{-3} can be assumed. This favored an exceptionally strong gravitational
805 instability that initially possibly triggered variable subsidence rates during the
806 deposititon of the MS that prefigured the synclines. Our results suggest that solid state
807 upward doming and exhumation of the crystalline basement was coeval with repeated
808 sagduction of the Minas Supergroup. The mostly brittle character of regional
809 deformation in the granites and gneisses suggests that much of the shear concentrated
810 in steeply dipping shales and Fe-rich layers of the MS and along lithological
811 boundaries from the synclinal limbs, whereas nearly flat-lying strata affected by
812 moderate deformation are observed from the hinges of synclines. The lack of both
813 temperature and pressure increase towards the center of the domes originally buried at
814 12 to 15 km depths, and the ages of metamorphic minerals in the east (480-490 Ma)
815 indicate that the building up the « dome and keel » province of the Quadrilátero
816 Ferrífero relates to the Early Paleozoic tectono-metamorphic event, as concluded by
817 Chauvet et al. (2001). The large-scale X-shape geometry of the MS synclines with two
818 triple junctions precludes a coherent uniform direction of shortening and is more in
819 agreement with dominant vertical tectonics. However, the similar pressure and

temperature conditions for the last metamorphic event in basement and cover synclines implies that the tectonic burial of the eastern Quadrilátero Ferrífero requires the overload of several km represented by allochtonous units of the external Araçuaí nappes. Such allochtonous interpretation first proposed by Romano (1989) and Chemale et al. (1994) fits with the preservation of allochtonous units in the Ouro Branco synform. The tectonic interpretation for the Quadrilátero Ferrífero (Figure 10) postulates a NW-directed blind thrust at depths that merges north of the Serra do Curral-Sabará belt.

7.5. *General considerations and connection with the Araçuaí belt*

The question arises of what was driving the foreland contraction of the QFe 100 My after peak metamorphism in the Araçuaí orogen. The core of this hot orogen was subjected to high-temperature metamorphism (780-800°C) from 600 to 575 Ma (Cavalcante et al., 2018; Vauchez et al., 2019). The $^{40}Ar/^{39}Ar$ dates obtained on amphibole (505 Ma), muscovite (484 Ma), and biotite (482 Ma) bythe latter authors indicate that the Araçuaí crust remained above the Ar closure temperature for hornblende and micas for nearly 100 Ma years. Moreover, late- to post-kinematic charnockites were also intruded farther north at 504 ± 5 Ma (zircon SHRIMP concordia age, Gradim et al., 2014 and references therein). This suggests that hot and dry magmas of deep crustal origin are in part responsible for the rather long-lived thermal anomaly of this hot orogen.

Taking into account the space problem between the São Francisco and the Congo cratons, Fossen et al. (2020) recently invalidated an oceanic setting for the Araçuaí belt, as proposed by several authors (Pedrosa-Soares et al.,1992; 1998; Amaral et al. 2020 and references therein) and consider that this orogen did not form through the

incorporation of oceanic crust, but evolved above thinned continental crust. For Egydio-Silva et al. (2018), similar record of magmatism and timing of orogenic events and PT conditions during peak metamorphism evidence a continuity between the Araçuaí and the Ribeira belts. In contrast Heilbron et al. (2020) emphasize a complex evolution of magmatic arcs for the Ribeira belt and distinguish an inner magmatic arc system developed between ca. 650 and 595 Ma within a Paleoproterozoic microcontinent and a outer intra-oceanic magmatic arc system as old as 860-760 Ma. It is worth noting that the metamorphic regime and metamorphic field gradients all along the external western segment of the Araçuaí belt display east-dipping inverted isograds, a situation that is in part similar to the Himalayan range. Along an E-W transect 150 km to the north of the QFe, Peixoto et al. (2015) report an east-dipping Barrovian-type unit (widespread occurrence of kyanite and staurolite T= 550°C and P around 8 kbar) as depicted east of Mariana in section 5.4, overlain by a distinct low-pressure cordierite-sillimanite unit. Two fundamental features of the Araçuaí belt must also be highlighted: i/ the existence of a horizontal, thick unit of kinzigites that represent the upper crystalline nappe of the eastern domain; and ii/ a deeper external thick band of high-temperature mylonites that delimits the western domain (Vauchez et al., 2019). These features strongly suggest a Himalayan-size nappe system (Figure 12 of Vauchez et al. 2019) and the complete allochthonous nature of the hot part of the Araçuaí belt.

In the case of the central Himalaya, the emplacement of the Greater Himalayan sequence (GHS) on top of the Lesser Himalaya units relates to the progressive activation of top-to-the S nearly horizontal shear zones from 42 to 12 Ma (Carosi et al., 2016) with spatial and temporal discontinuities (Wang et al., 2016; Iaccarino et al., 2017). For Parson et al. (2016), the GHS formed as a partially molten, rheologically

weak subhorizontal layer that flowed southward relative to the upper and lower crust. This "channel flow" progressively evolved towards wedge extrusion and to a system of thrust stacking/duplexing. Regarding the Araçuaí belt, further structural/kinematic analysis and geo/thermo-chronological investigations spanning a range of cooling conditions are needed to test a possible model of channel flow as proposed by Cavalcante et al. (2018).

8. Conclusions

In line with the classical interpretations of Dorr (1969), an angular stratigraphic unconformity is clearly present at the base of the Minas Supergroup deposited after deep erosion of the Archean basement of the QFe. Most thermal aureoles observed in the Rio das Velhas Supergroup and Minas Supergroup represent hornfelses, most of them lacking syn-kinematic features. Monazite and titanite of Orosirian age (2048-2034 Ma, Carvalho et al., 2017) relate to the reheating of the Archean basement and to the emplacement of pegmatites and of granitic stocks best recorded in the Sabará Group, at 12-15 km depths in an extensional setting. Though some high-temperature mineral assemblages from the thermal aureoles are locally slightly retrogressed, a pervasive tectono-metamorphic overprint produced the same superimposed greenschist facies cleavage with the same kinematic indicators in all metasedimentary rocks ranging in age from Archean to Ediacaran at least in the eastern part of the Quadrilátero Ferrífero. Regional temperatures around 420°C and pressures of 4.5 to 5 kbar are constrained by the coexistence of pyrophyllite and kyanite in aluminous metasediments, and by phengite-biotite-microcline in quartz-feldspathic rocks. This low-temperature tectono-metamorphic regime was apparently uniform in the domes

and the keels. It is concluded that tectonic burial of the eastern Quadrilátero Ferrífero was achieved as the result of tectonic overload of the west-verging external Arçuaí nappes. The late stage of this Ediacaran to Cambro-Ordovician collision, that affected the whole of eastern Brazil, produced the deformation and greenschist facies overprint in the rigid cratonic foreland of the Araçuaí orogen, including the basement dome-and-keel structures and final sagduction of their sedimentary cover. Dominant steeply dipping mineral and stretching lineations in the domes indicate moderate sub-vertical elongation achieved in solid-state conditions. It is concluded that the cold upward to NW-directed oblique extrusion of the Bação dome relates to the combined effects of west to northwest-directed blind thrusting at depths and a high buoyancy contrast estimated ≥ 0.4 g. cm^{-3} between the Archean quartz-feldspathic rocks and the metasedimentary pile preserved in the keels, due to the abundance and thickness of Fe-rich horizons. With the data currently available, it is reasonable to propose that (1) crystalline units from the core of the Araçuaí belt were expelled westward, resulting in progressive burial and reheating of the São Francisco craton and its cover during the early Paleozoic, and (2) delamination of the lower crust assisted by repeated hot and dry magmatism of deep crustal origin may represent a possible scenario to explain the significant width of the QFe contraction zone in the foreland of the Araçuaí orogen.

References

Aguilar, C., Alkmim, F.F., Lana, C., Farina, F., 2019. Palaeoproterozoic assembly of the São Francisco craton, SE Brazil: new insights from U-Pb titanite and monazite dating. Precambrian Research 289, 95-115.

Alkmim, F. F. and Marshak, S., 1998. Transamazonian Orogeny in the Southern São Francisco Craton Region, Minas Gerais, Brazil: evidence for Paleoproterozoic collision and collapse in the Quadrilátero Ferrífero. Precambrian Research 90, 29-58.

Alkmim, F.F., Martins-Neto, M.A. 2012. Proterozoic first-order sedimentary squences of the São Francisco craton, eastern Brazil. Marine and Petroleum Geology 33, 127-139.

Almeida Abreu, P.A., Pflug, R.,1994. The geodynamic evolution of the southern Serra do Espinhaço, Minas Gerais, Brazil. Zbl. Geol. Palaont. Teil I: 1, 21-44.

Almeida Abreu, P.A., Pflug, R., Schorscher, H.D. 1992. Cover/basement relationships in the southern Serra do Espinhaço, Minas Gerais, Brazil. Zbl. Geologishe Paläontologische I: 1749-1760.

Ávila, C.A., Teixeira, W., Cordani, U.G., Veloso Moura, C.A., Pereira, R.M., 2010. Rhyacian (2.23 – 2.20 Ga) juvenile accretion in the southern São Francisco Craton, Brazil: Geochemical and isotopic evidence form the Serrinha magmatic suite, Mineiro belt. J. S. Am. Earth Sci. 29, 464–482.

Babinski, M., Chemale Jr., F., Van Schumus, W.R., 1995. The Pb/Pb age of the Minas Supergroup carbonate rocks, Quadrilátero Ferrífero, Brazil. Precambr. Res. 72, 235–245.

Barbosa, N.S., Teixeira, W., Ávila, C.A., Montecinos, P.M., Bongiolo, E.M. 2015. 2.17–2.10 Ga plutonic episodes in the Mineiro belt, São Francisco Craton, Brazil: U-Pb ages, geochemical constraints and tectonics. Precambrian Research 270, 204-225.

Parra-Avila, L.A, Kemp, A.I.S., Fiorentini, M.L., Belousova E., Baratoux, L., Block, S., Jessell, M., Bruguier, O., Graham C., Begg, G.C., Miller, J., Davis, J., McCuaig, C., 2017. The geochronological evolution of the Paleoproterozoic Baoulé-Mossi domain of the Southern West African Craton. Precambrian Research 300, 1-27.

Brueckner, H.K., Cunningham, D., Alkmim, F., Marshak, S. 2000. Tectonic implications of Precambrian Sm-Nd dates from the southern São Francisco craton and adjacent Araçuaí and Ribeira belts, Brazil. Precambrian Research 99, 255-269.

Caggianelli, A., Ranalli, G., Lavecchia, A., Liotta, D., Dini, A. 2014. Post-emplacement thermo-rheological history of a granite intrusion and surrounding rocks: the Monte Capanne pluton, Elba Island, Italy. In: Llana-Fúnez, S., Marcos, A. & Bastida, F. (eds): Deformation Structures and Processes within the Continental Crust. Geological Society, London, Special Publications, 394.

Carosi, R., Montomoli, C., Iacarino, S., Massonne, H.J., Rubatton, D., Langone, A., Gemignani, L., Visona, D., 2016). Middle to late Eocene exhumation of the Greater Himalayan Sequence in the Central Himalayas: Progressiver accrtetion from the Indian plate. Geological Society of America Bulletin 128, 1571-1592.

Carvalho, B.B., Janasi, V.A., Sawyer, E.V. 2017. Evidence for Paleoproterozoic anatexis and crustal reworking of Archean crust in the São Francisco Craton, Brazil: A dating and isotopic study of the Kinawa migmatite. Precambrian Research 291, 98-118.

Cavalcante, C., Hollanda, M.H.B.M., Vauchez, A., Kawata, M., 2018. How long can the middle crust remain partially molten during orogeny? Geology 46, 839–842.

Cavalcante, C., Fossen, H., de Almeida, R.P., Hollanda, M.H.B.M., Egydio-Silva, M., 2019. Reviewing the puzzling intracontinental termination of the Araçuaí-West Congo orogenic belt and its implications for orogenic development. Precambrian Research 322, 85–98.

Cavalcante, G.C.G., Egydio-Silva, M., Vauchez, A., Camps, P., Oliveira, E., 2013. Strain distribution across a partially molten middle crust: insights from the AMS mapping of the Carlos Chagas Anatexite, Araçuaí belt (East Brazil). Journal of Structural Geology 55, 79–100.

Cederberg, J.,2013. U-Pb dating of the Para de Minas dyke swarm in the São Francisco craton (Brazil) - three generations in a single swarm. PhD thesis Lund, Sweeden (unpublished).

990 Chardon, D., Choukroune, P. 1996. Strain patterns, décollement and incipient
991 sagducted greenstone terrains in the Archaean Dharwar craton (south India). Journal of
992 Structural Geology 18, 991-1004.
993
994 Chauvet, A., Piantone, P., Barbanson, L., Nehlig, P., Pedroletti, I., 2001. Gold deposit
995 formation during collapse tectonics: structural, mineralogical, and fluid inclusions
996 constraints in the Ouro Preto gold mines, Quadrilátero Ferrífero, Brazil. Economic
997 Geology 96, 25-48.
998
999 Chaves, A.O., Goulart, L.E.A., Coelhoa, R.M., Miranda, D.M., Aranda, D.A., Ramos,
1000 S.L., 2019. High-pressure eclogite facies metamorphism and decompression melting
1001 recorded in Paleoproterozoic accretionary wedge adjacent to probable
1002 ophiolite from Itaguara (southern São Francisco Craton - Brazil). Journal of South
1003 American Earth Sciences 94, 102226
1004
1005 Chemale, F., Rosière, C.A., Endo, I. 1994. The tectonic evolution of the Quadrilátero
1006 Ferrífero, Minas Gerais, Brazil. Precambrian Research 65, 25-54.
1007
1008 Choukroune, P., Bouhallier, H. and Arndt, N.T., 1995. Soft lithosphere during periods
1009 of Archaean crustal growth or crustal reworking. *In* M.P. Coward, & A.C. Ries (eds)
1010 Early Precambrian Processes, Geological Society Special Publication 95, 67-86.
1011
1012 Cruz, S.C., Figueiredo Barbosa, J.S., Pinto, M.S., Peucat, J.J., Paquette, J.L., Santos de
1013 Souza, J., de Souza Martins, V., Júnior, F.C., Carneiro, M.A., 2016. The Siderian-
1014 Orosirian magmatism in the Archean Gavião Paleoplate, Brazil: U-Pb geochronology,
1015 geochemistry and tectonic implications, Journal of South American Earth Sciences.
1016
1017 Cutts, K., Lana, C., Alkmim, F., Farina, F., Moreira, H., Voelha, V. 2019.
1018 Metamorphism and exhumation of basement gneiss domes in the Quadrilátero
1019 Ferrífero: Two stage dome-and-keel evolution?. Geoscience Frontiers,
1020 https://doi.org/10.1016/j.gsf.2019.02.009
1021

Dorr, J.V.N., II, 1969. Physiographic, stratigraphic and structural development of the Quadrilátero Ferrífero, Minas Gerais. U.S. Geological Survey Professional Paper 641-A, 110 p.; Geological map of the Quadrilátero Ferrífero 1 : 150.000, DNPM/USGS.

Dumont, T. 1988. Late-early Jurassic evolution of the western Alps and of their European foreland; initiation of the Tethys rifting. Bulletin de la Société géologiquee de France 8, 601-611.

Dutra, L.F., Martins, M., Lana, C. 2019. Sedimentary and U-Pb detrital zircons provenance of the Paleoproterozoic Piracicaba and Sabará groups, Quadrilátero Ferrífero, Southern São Francisco craton, Brazil. Brazilian Journal of Geology 49, e20180095.

Egydio-Silva, M., Vauchez, A., Fossen, H., Gonçalves Cavalcante, G.C., Xavier, B.C., 2018. Connecting the Araçuaí and Ribeira belts (SE – Brazil): Progressive transition from contractional to transpressive strain regime during the Brasiliano orogeny. Journal of South American Earth Sciences 86, 127–139.

Egli, D., Mancktelov, N., Spikings, R. 2017. Constraints from $^{40}Ar/^{39}Ar$ geochronology on the timing of Alpine shear zones in the Mont Blanc□Aiguilles Rouges region of the European Alps. Tectonics 36, doi.org/10.1002/2016TC004450.

Endo, I., Fonseca, M.A. 1992. Sistema de cisalhamento Fundão-Cambotas no Quadrílatero Ferrífero, MG: geometria e cinemática. Revista da Escuola das Minas, Ouro Preto, Brazil 45, 28-31.

Farina, F., Albert, C., Lana, C. 2015. The Neoarchean transition between medium- and high-K granitoids: Clues from the Southern São Francisco craton (Brazil). Precambrian Research 266, 375-394.

Fossen, H., Cavalcante, C., Konopásek, J., Meira, T., Paes de Almeida, R., Hollanda, B.M., Trompette, R., 2020. A critical discussion of the subduction-collision model for the Neoproterozoic Araçuaí-West Congo orogen. Precambrian Research 343, 105715.

1056 François, C, Philippot, P., Rey, P., Rubatto, D. 2014. Burial and exhumation during
1057 Archean sagduction in the East Pilbara Granite-Greenstone Terrane. Earth and
1058 Planetary Science Letters 396, 235-251.
1059
1060 Gomes, N.S., Muller, G., 1987. Caracterização química de Parageneses de Minerais de
1061 Alto Grau Metamórfico no Complexo Bação, Quadrilátero Ferrífero. Revista da
1062 Escola das Minas, Ouro Preto, Brazil, 40, 25-36.
1063
1064 Gradim, C., Roncato, J., Pedrosa-Soares, A.C., Cordani, U., Dussin, J., Alkmim, F.F.,
1065 Queiroga, G., Jacobsohn, T., da Silva, L.C., Babinski, M. 2014. The hot back-arc zone
1066 of the Araçuaí orogen, Eastern Brazil: from sedimentation to granite generation.
1067 Brazilian Journal of Geology 44, 155-180.
1068
1069 Gratier, J. M., Vialon, P. 1980. Deformation pattern in a heterogeneous material:
1070 folded and cleaved sedimentary cover immediately overlying a crystalline basement,
1071 Oisans, French Alps. Tectonophysics 65, 151-180.
1072
1073 Heilbron, M., Valeriano, C.M., Peixoto, C., Tupinamba, M., Neubauer, F., Dussin, I.,
1074 Corrales, F., Bruno, H., Lobato, M., Almeida, J.C.H., Eirado Silva, L.G. 2020.
1075 Neoproterozoic arc systems of the central Ribeira belt, SE-Brazil, in the context of the
1076 West-Gondwana pre-collisional history: A review. Journal of South American Earth
1077 Sciences 103, 102710.
1078
1079 Herz, N ., 1978. Metamorphic rocks of the Quadrilátero Ferrífero, Minas Gerais,
1080 Brazil. US Geological Survey Prof. Paper 641-C Ci-C81.
1081
1082 Hippertt, J.F., 1998. Breakdown of feldspar, volume gain and lateral mass transfer
1083 during mylonitization of granitoid in a low metamorphic grade shear zone. Journal of
1084 Structural Geology 20, 175-193.
1085
1086 Hippertt, J., Davis, B. 2000. Dome emplacement and formation of kilometre-scale
1087 synclines in a granite-greenstone terrain (Quadrilátero Ferrífero, southeastern Brazil).
1088 Precambrian Research 102, 99-121.
1089

1090 Iaccarino S., Montomoli C., Carosi R., Massonne H.-J, Langone A., Visonà, D. 2015.
1091 Pressure-temperature-deformation path of kyanite-bearing migmatitic paragneiss in
1092 the Kali Ganfdakivalley (central Nepal): Investigation of late Eo ene-early Oligocene
1093 melting process. Lithos 231, 03-121
1094
1095 Jordt-Evangelista, H., Alkmim, F.F., Marshak, S. 1992. Metamorfismo progressivo e a
1096 ocorrência dos três plimorpfos de Al2SiO5 (cianita, andaluzita e sillimanita) na
1097 Formação Sabara em Ibirité, Quadrilátero Ferrífero, M. G. Revista da Escuola de
1098 Minas, Ouro Preto, Brazil, 45, 157-160.
1099
1100 Koglin, N., Zeh, A., Cabral, A.R., Gomes Jr., A. A. S., Vasconcelos, A., Corrêa Neto,
1101 A. V., Brunetto W. J., Galbiatti, H. 2014. Depositional age and sediment source of the
1102 auriferous Moeda Formation, Quadrilátero Ferrífero of Minas Gerais, Brazil: New
1103 constraints from U–Pb–Hf isotopes in zircon and xenotime.
1104 Precambrian Research 255, 96-108.
1105
1106 Lana, C., Alkmim, F.F., Armstrong, R., Schotz, R., Romano, R., Nalini, H.A. 2013.
1107 The ancestry and magmatic evolution of Archean TTG rocks of the Quadrilátero
1108 Ferrífero province, southeast Brazil. Precambrian Research 231, 157-173.
1109
1110 Lin, S. 2005. Synchronous vertical and horizontal tectonism in the Neoarchean:
1111 Kinematic evidence from a synclinal keel in the northwestern Superior craton, Canada.
1112 Precambrian Research 139, 181-194.
1113
1114 Machado, N., Carneiro, M.A., 1992. U-Pb evidence of late Archean tectono-thermal
1115 activity in the southern São Francisco shield, Brazil. Canadian Journal of Earth
1116 Sciences 29, 2341-2346.
1117
1118 Machado, N., Noce, C.M., Ladeira, E.A., Belo de Oliveira, O.A., 1992. U-Pb
1119 geochronology of Archean magmatism and Proterozoic metamorphism in the
1120 Quadrilátero Ferrífero, southern São Francisco Craton, Brazil. Geological Society of
1121 American Bulletin 104, 1221-1227.
1122
1123 Machado, N., Gauthier, G. 1996. Determination of 207Pb/206Pb ages on zircon and

monazite by laser-ablation ICPMS and application to the study of sedimentary provenance and metamorphism in southeastern Brazil. Geochimica Cosmochimica Acta 60, 5063-5073.

Machado, N., Schrank, A., Noce, C. M., Gauthier, G. 1996. Ages of detrital zircon from Archean-Paleoproterozoic sequences : implications for Greenstone Belt setting and evolution of a Transamazonian foreland basin in the Quadrilátero Ferrífero, southeast Brazil. Earth Planetary Sciences Letters 141, 259-276.

Marshak, S., Alkmim, F.F., Jordt-Evangelista, H. 1992. Proterozoic crustal extension and the generation of dome-and-keel structure in an Archaean granite-greenstone terrane. Nature 357, 491-493.

Marshak, S., Tinkham, D., Alkmim, F., Brueckner, H., Bornhost, T. 1997. Dome-and-keel provinces formed during Paleoproterozoic orogenic collapse-core complexes, diapirs, or neither?: Examples from the Quadrilátero Ferrífero and the Penokean orogen. Geology 25, 415-418.

Martinez Dopico, C.I, Lana, C., Moreira, H.S., Cassino, L.F., Alkmim, F.F. 2017. U-Pb ages and Hf-isotope data of detrital zircons from the late Neoarchean-Paleoproterozoic Minas Basin, SE Brazil. Precambrian Research 291, 143-161.

Massonne, H.J., Schreyer, W., 1987. Phengite geobarometry based on the limiting assemblage with K-feldspar, phlogopite, and quartz. Contributions Mineralogy and Petrology 96, 212-224.

Moreira, H., Lana, C., Nalini, H.A. 2016. The detrital record of an Archean convergent basin in the Southern São Francisco craton, Brazil. Precambrian Research 275, 84-99.

Noce, C. M. (2000). Geochronology of the Quadrilátero Ferrífero: a review. Geonomos, 8, 15-23.

1157 Parmenter, A.C., Lin, S, Corkey, M.T. 2006. Structural evolution of the Cross Lake
1158 greenstone belt in the northwestern Superior Province, Manitoba: implications for
1159 relationship between vertical and horizontal tectonism. Canadian Journal of Earth
1160 Sciences 43, 767-787.
1161
1162 Parra-Avila, L.A, Kemp, A.I.S., Fiorentini, M.L., Belousova E., Baratoux, L., Block,
1163 S., Jessell, M., Bruguier, O., Graham C., Begg, G.C., Miller, J., Davis, J., McCuaig,
1164 C., 2017. The geochronological evolution of the Paleoproterozoic Baoulé-Mossi
1165 domain of the Southern West African Craton. Precambrian Research 300, 1-27.
1166
1167 Parson, A.J., Law, R.D., Lloyd, G.E., Phillips, R.J., Searle, M.P. 2016. Thermo-
1168 kinematic evolution of the Annapurna-Dhaulagiri Himalaya, central Nepal: the
1169 Composite Orogenic System. Geochemistry Geophysics Geosystems AGU Publication
1170 17, 1511-1539.
1171
1172 Peixoto, E., Pedrosa-Soares, A. C., Alkmim, F. F., Dussin, I.A. 2015. A suture-related
1173 accretionnary wedge formed in the NeoproterozoicAraçuaí orogen(SE Brazil) during
1174 the Western Gondwana assembly. Gondwana Research 27, 878-896.
1175
1176 Rapp, R.P., Watson, E.B., 1995. Dhydration melting of metabasalt at 8–32 kbar:
1177 implications for continental growth and crust-mantle recycling. Journal of Petrology
1178 36, 891– 931.
1179
1180 Reis, L.A., Martins-Neto, M. A., Gomes, N.S., Endo, I., Jordt-Evangelista, H., 2002.
1181 A bacia de antepaís Paleoproterozóica Sabará, Quadrilátero Ferrífero, Minas Gerais.
1182 Revista Brasileira de Geociências 32, 27-42.
1183
1184 Rey, P.F., Vanderhaeghe, O., Teyssier, C., 2001. Gravitational collapse of the
1185 continental crust: definition, regimes and modes. Tectonophysics 342, 435–449.
1186
1187 Rolland, Y, Cox, S., Boullier, A.M., Pennachioni, G., Manktelow, N. 2003. Rare
1188 earth and trace elements mobility in mid-crustal shear zones: insights from the Mont
1189 Blanc Massif (Western Alps). Earth and Planetary Science Letters 214, 203-219.
1190

1191 Rolland, Y., Rossi, M., Cox, S. F., Corsini, M., Mancktelow, N., Pennacchioni, G.,
1192 Fornari, M., Boullier, A.M. 2008. 40Ar/39Ar dating of synkinematic white mica:
1193 insights from fluid-rock reaction in low-grade shear zones (Mont Blanc Massif) and
1194 constraints on timing of deformation in the NW external Alps. Geological Society,
1195 London, Special Publications 2008, v. 299, 293-315.
1196
1197 Romano, A.W. 1989. Evolution tectonique de la région NW du Quadrilatère Ferrifère-
1198 Minas Gerais, Brésil. Thèse de Doctorat, Université de Nancy I, France, 259 p.
1199
1200 Romano, R., Lana, C., F.F. Alkmim, Stevens, G., Armstrong, R. 2013. Stabilization of
1201 the southern portion of the São Francisco craton, SE Brazil, through a long-lived
1202 period of potassic magmatism. Precambrian Research 224, 143- 159.
1203
1204 Rosière, C. A., Spier, C. A., Rios, F. J., Suckau, V. E. 2008. The itabirites of the
1205 Quadrilátero Ferrífero and related high-grade iron ore deposits: an overview. Society
1206 of Economic Geologists SEG Reviews 15, 223-254.
1207
1208 Rushmer, T., 1991. Partial melting of two amphibolites. Contrasting results under
1209 fluid-absent conditions. Contributions to Mineralogy and Petrology 107, 41-59.
1210
1211 Sandiford, M., M. J., Van Kranendonk, S. Bodorkos, 2004. Conductive incubation and
1212 the origin of dome-and-keel structure in Archean granite-greenstone terrains: A model
1213 based on the eastern Pilbara Craton, Western Australia, Tectonics, 23, TC1009,
1214 doi:10.1029/ 2002TC001452.
1215
1216 Sanglard, J. C. D., Rosière, C.A., Santos, J. O. S., McNaughton, N. J., Fletcher, I. R.,
1217 2014. A estrutura do segmento oeste da Serra do Curral, Quadrilátero Ferrífero, e o
1218 controle tectônico das acumulações compactas de alto teor em Fe. Revista do Instituto
1219 de Geociências - USP São Paulo 14, 81-95.
1220
1221 Schorscher, H.D., Santana, F. C., Polonia, J.C, Moreira, ,J.M. 1982. Quadrilátero
1222 Ferrífero – Minas Gerais state : Rio das Velhas greenstone belt and Proterozoic rocks.
1223 International Symposium of Archean Early Proterozoic Geologic Evolution and

Metallogenesis. Excursion annex, 3-11 Sept. 1982, Salvador, Ba, Brazil, 44p.

Silva, A.M., Chemale Jr F., Kuyumjian, R.M., Heaman, L. 1995. Mafic dike swarms of Quadrílatero Ferrífero and Southern Espinhaço, Minas Gerais. Revista Brasileira de Geosciências 25, 124-137.

Teixeira, W., Cordani, U. G., Nutman, A. P., Sato, K., 1998. Polyphase Archean evolution in the Campo Belo metamorphic complex, Southern São Francisco Craton, Brazil: SHRIMP U-Pb zircon evidence. Journal of South American Earth Sciences, 11, 279-289.

Teixeira, W., Ávila, C.A. , Dussin, I.A., Corrêa Neto, A.V., Bongiolo, E.M., Santos J.O., Barbosa, N.S. 2015. A juvenile accretion episode (2.35–2.32 Ga) in the Mineiro belt and its role to the Minas accretionary orogeny: Zircon U–Pb–Hf and geochemical evidences. Precambrian Research 256, 148–169.

Uhlein, G.J., Uhlein A., Stevenson, R., Halverson, G. P., Caxito, F., Cox, G. M. 2017. Early to late Ediacaran conglomeratic wedges from a complete foreland basin cycle in the southwest São Francisco Craton, Bambuí Group, Brazil. Precambrian Research 299, 101-116.

Teyssier , C., Whitney, D. 2002. Gneiss domes and orogeny. Geology 30, 1139-1142.

Vauchez, A., Hollanda, M.H. B.M., Monié, P., Mondou, M., Egydio-Silva, M. 2019. Slow cooling and crystallization of the roots of the Neoproterozoic Araçuaí hot orogen (SE Brazil): Implications for rheology, strain distribution, and deformation analysis. Tectonophysics 766, 500-518.

Wang, J.M., Zhang, J.J., Liu, K., Zhang, B., Wang, X.X., Raid, S.M., Scheltens, M. 2016. Spatial and temporal evolution of tectonometamorphic discontinuities in the central Himalaya: Constraints from P-T paths and geochronology. Tectonophysics 41-69.

1257 Whitney, D., Teyssier, C., Vanderhaeghe, O., 2004. Gneiss domes and crustal flow.
1258 Geological Society of America Special Paper 380, 33.
1259
1260 Whitney, D., Teyssier, C., Rey, P., Buck, R.W. 2013. Continental and oceanic core
1261 complexes. Geological Society of America Bulletin 125, 273-298.
1262
1263 Xu, G., Will, T.M., Powell, R., 1994. A calculated petrogenetic grid for the system
1264 K2O-FeO-MgO-Al2O3-SiO2-H2O, with particular reference to contact
1265 metamorphosed pelites. Journal of Metamorphic Geology 12, 99–119.

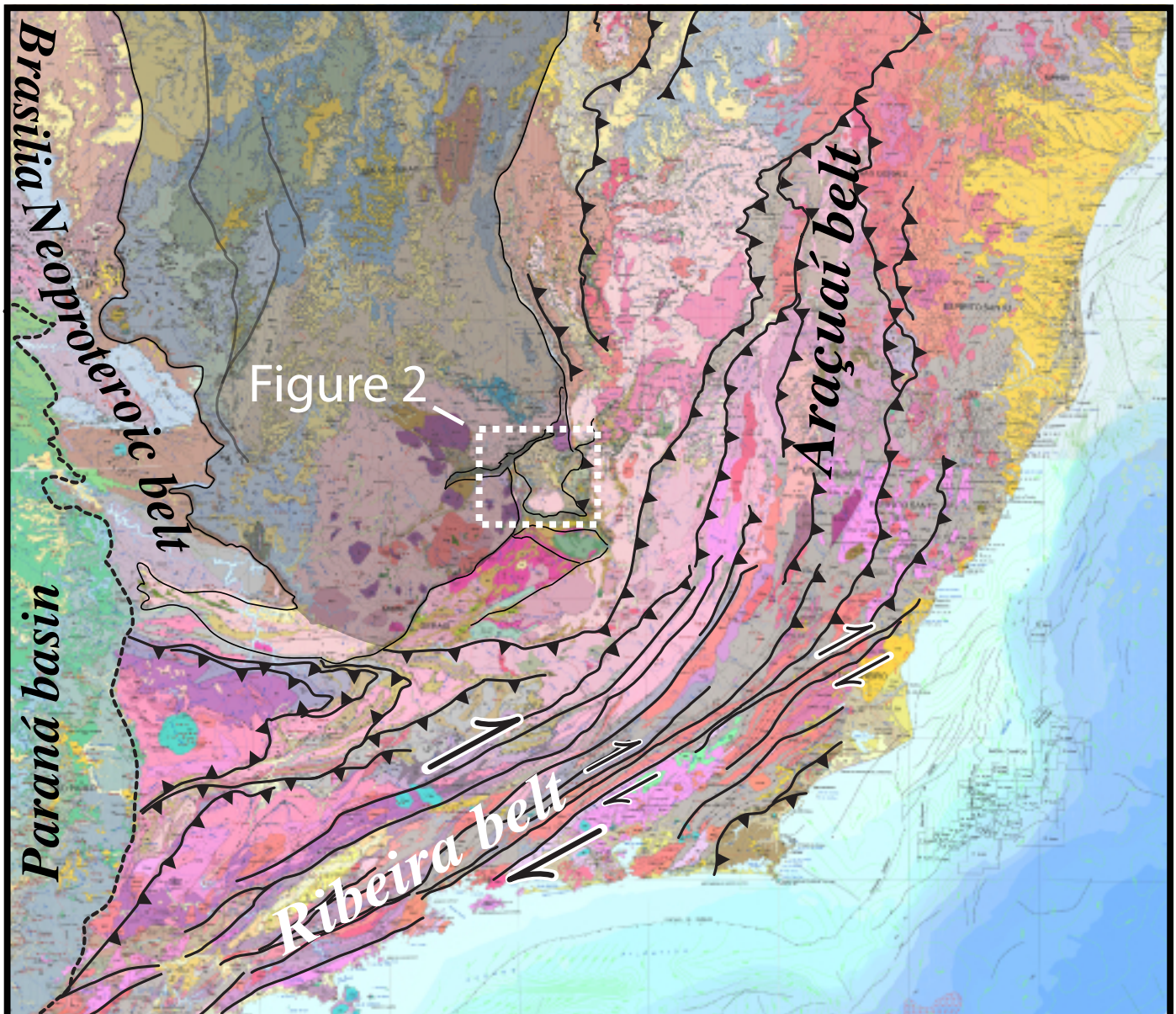
Brasília Neoproterozoic belt
Paraná basin
Figure 2
Araçuaí belt
Ribeira belt

Figure 1

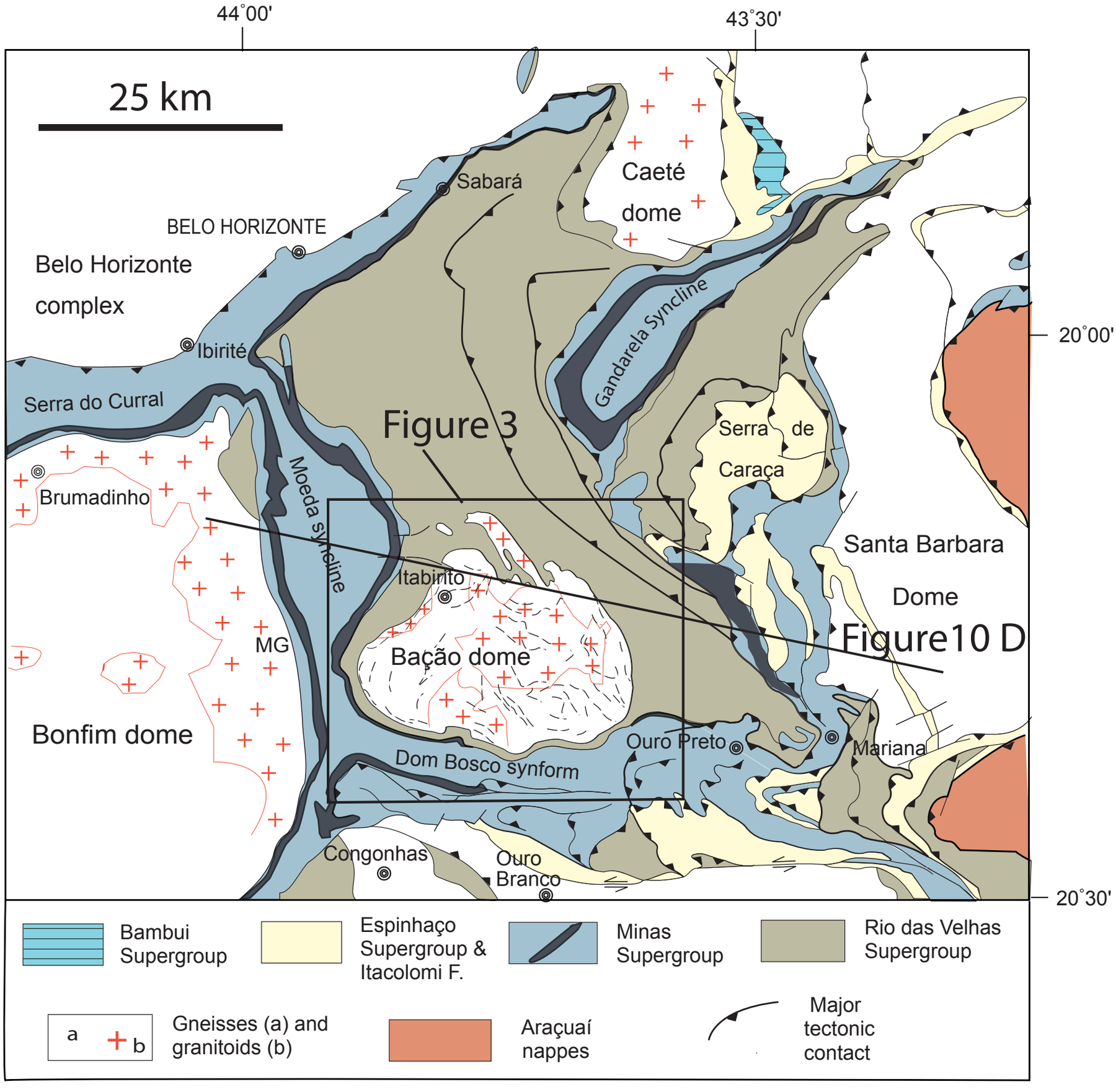
44˚00'
43˚30'
25 km
Sabará
Caeté
dome
BELO HORIZONTE
Belo Horizonte
complex
Ibirité
Gandarela Syncline
20˚00'
Serra do Curral
Figure 3
Serra de
Caraça
Brumadinho
Moeda syncline
Santa Barbara
Dome
Itabirito
Figure10 D
MG
Bação dome
Bonfim dome
Ouro Preto
Mariana
Dom Bosco synform
Congonhas
Ouro
Branco
20˚30'
Bambui
Supergroup
Espinhaço
Supergroup &
Itacolomi F.
Minas
Supergroup
Rio das Velhas
Supergroup
a
b
Gneisses (a) and
granitoids (b)
Araçuaí
nappes
Major
tectonic
contact

Figure 2

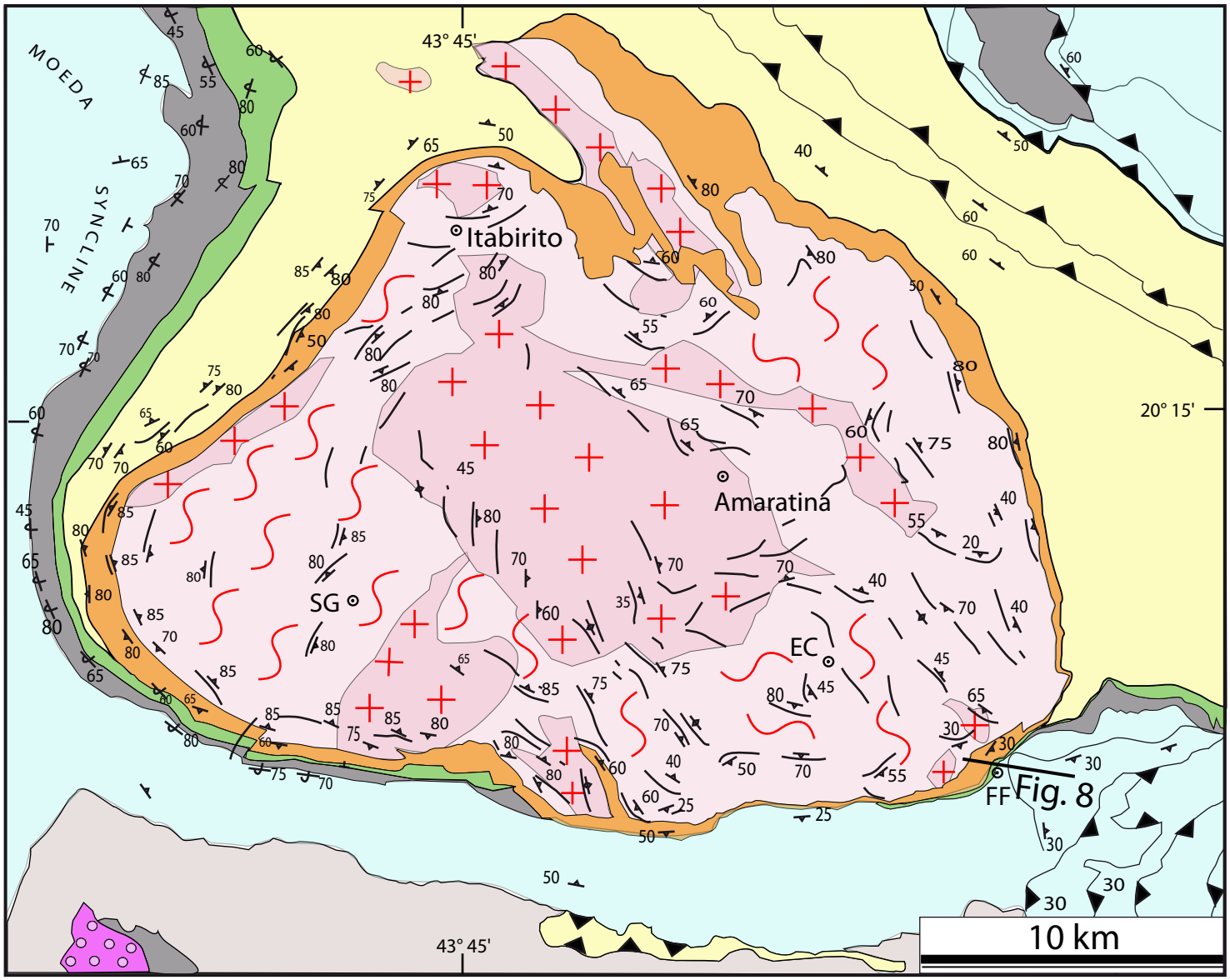
MOEDA
SYNCLINE
43° 45'
20° 15'
Itabirito
Amaratina
SG
EC
FF
Fig. 8
10 km
Minas Supergroup
Itacolomi Group (1.8-1.7 Ga)
Sabará Group (2.2- 2.04 Ga)
Undifferentiated MS (2.3-2.2 Ga)
Itabira Group (Fe formations, 2.4-2.3 Ga)
Moeda Quartzite (2.4 Ga)
Archean
Neoarchean granitoids (2.7-2.6 Ga)
a
b
Rio das Velhas Supergroup, greenschist facies (a) and amphibolite facies (b), (2.8-2.7 Ga)
Gneisses and anatexites, Archean foliation trajectories in black (≥ 2.8 Ga)
Sedimentary bedding
Foliation and cleavage
Major thrust

Figure 3

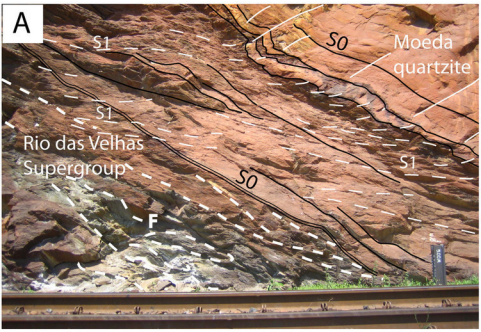
A
S1
S0
Moeda
quartzite
S1
Rio das Velhas
Supergroup
S0
S1
F


B
γ

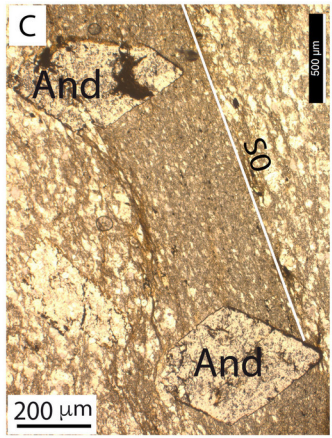
C
And
500 µm
S0
And
200 µm


D


E

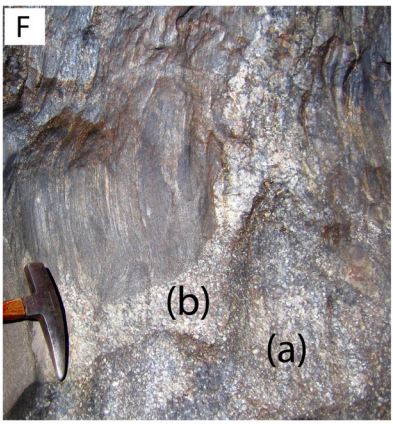
F
(b)
(a)


G
And

Figure 4

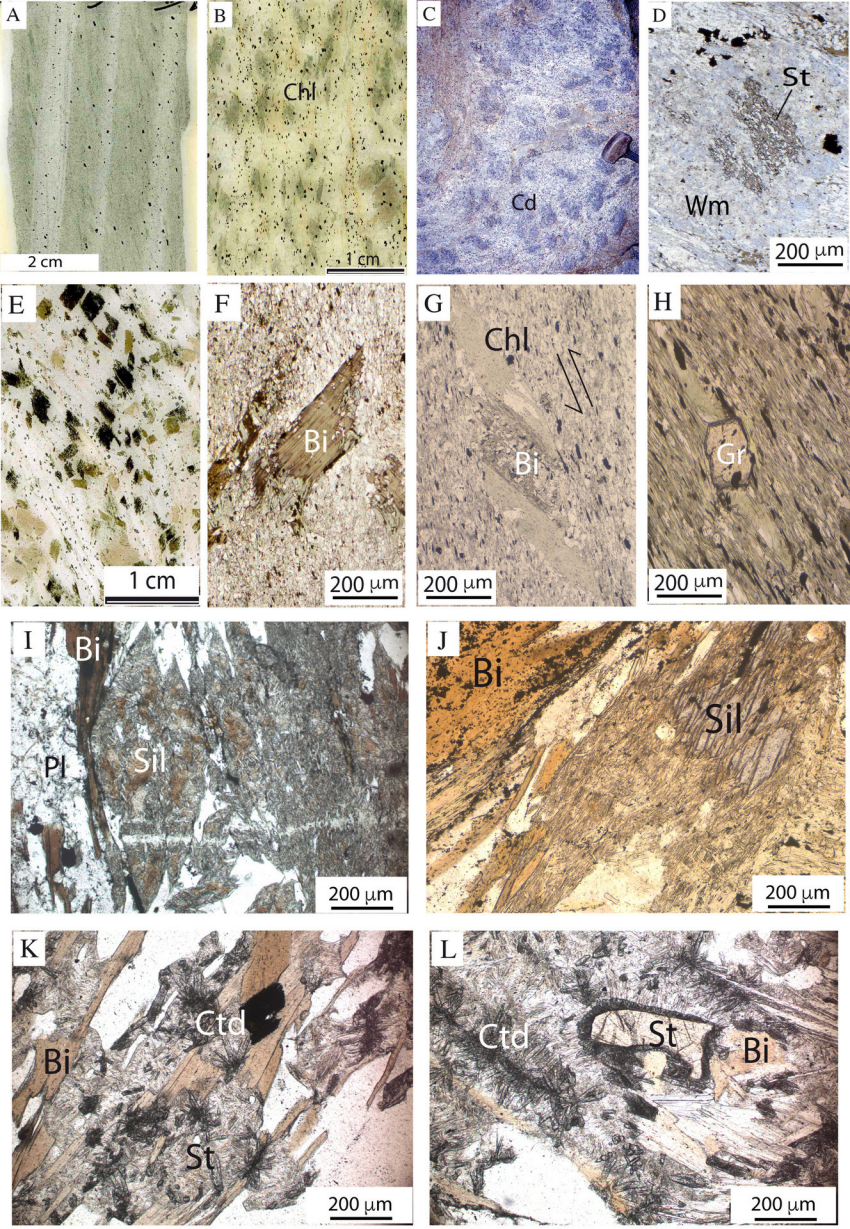
A
2 cm
B
Chl
1 cm
C
Cd
D
St
Wm
200 μm
E
1 cm
F
Bi
200 μm
G
Chl
Bi
200 μm
H
Gr
200 μm
I
Bi
Pl
Sil
200 μm
J
Bi
Sil
200 μm
K
Bi
Ctd
St
200 μm
L
Ctd
St
Bi
200 μm

Figure 5

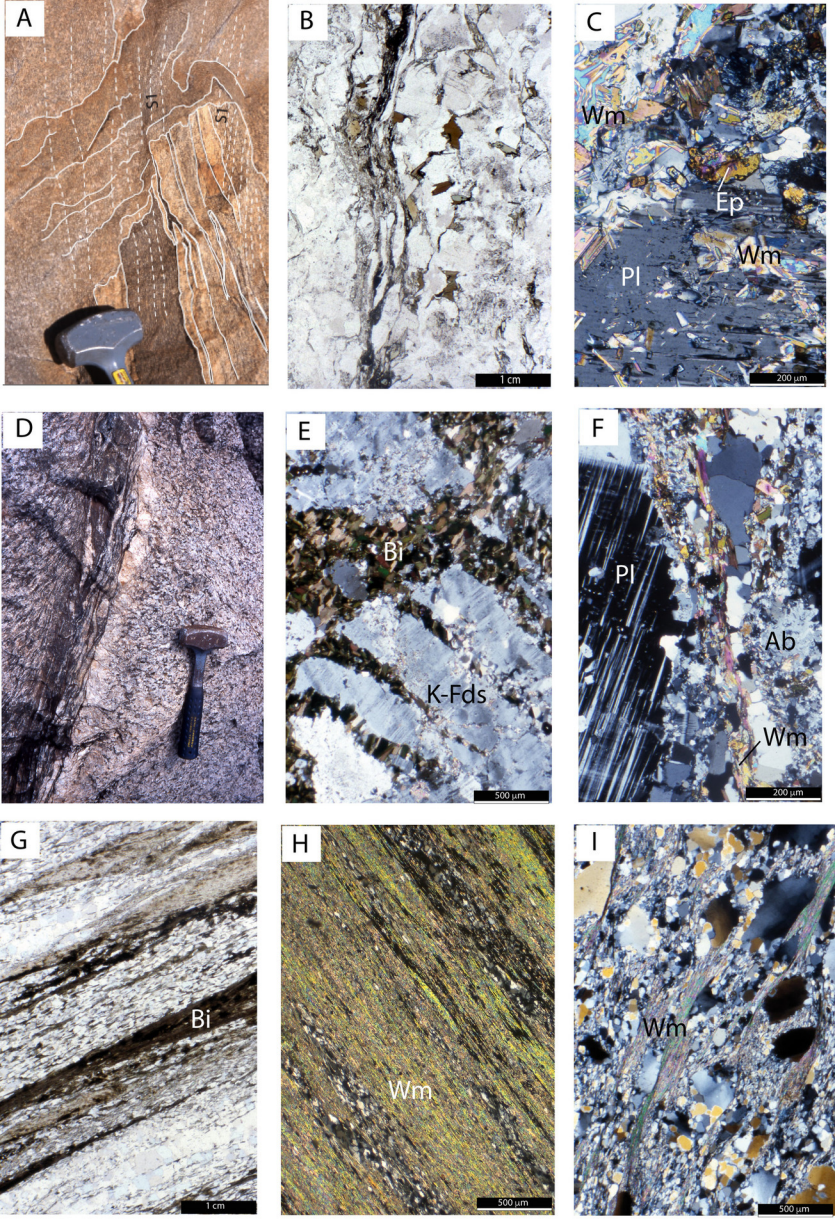
A
S1
S1
B
1 cm
C
Wm
Ep
Wm
Pl
200 µm
D
E
Bi
K-Fds
500 µm
F
Pl
Ab
Wm
200 µm
G
Bi
1 cm
H
Wm
500 µm
I
Wm
500 µm

Figure 6

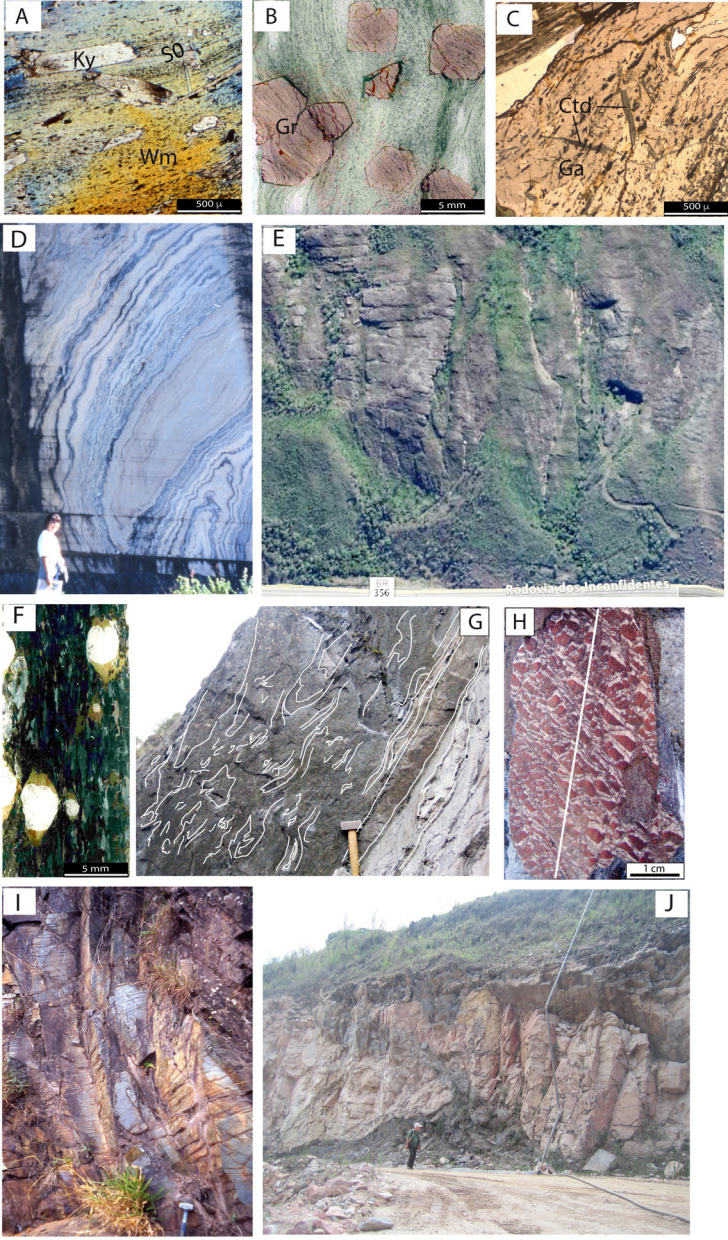
A
Ky
s0
Wm
500 µ
B
Gr
5 mm
C
Ctd
Ga
500 µ
D
E
356
Rodovias Inconfidentes
F
5 mm
G
H
1 cm
I
J

Figure 7

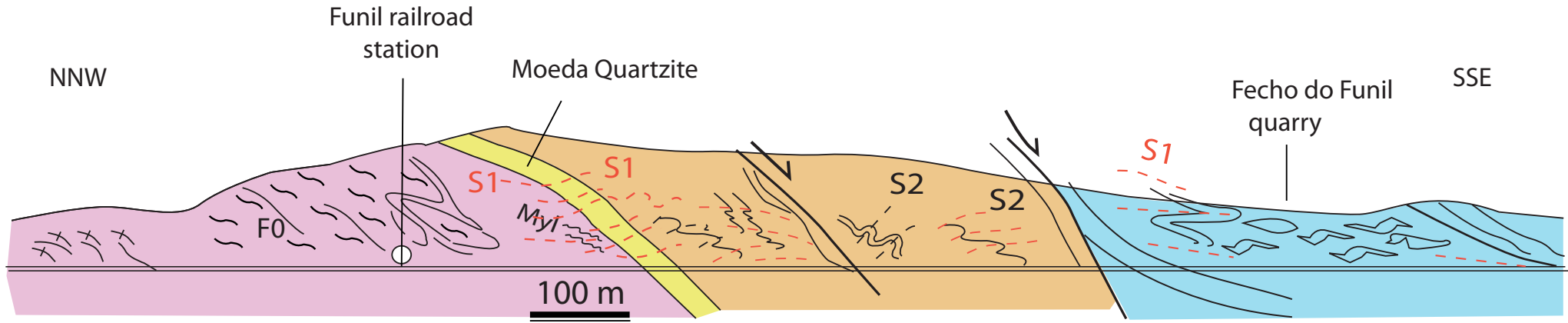
NNW
Funil railroad station
Moeda Quartzite
Fecho do Funil quarry
SSE
S1
S1
S2
S2
S1
Myl
F0
100 m
a
b
Foliated Archean granodiorite (a) and high-temperature metapelites of the Rio das Velhas Supergroup
Unconformable Moeda quartzite
Metapelites of the Batatal Formation
Undifferentiated metasedimentary rocks of the Fecho do Funil Formation (dolomite boudins are shown).

Figure 8

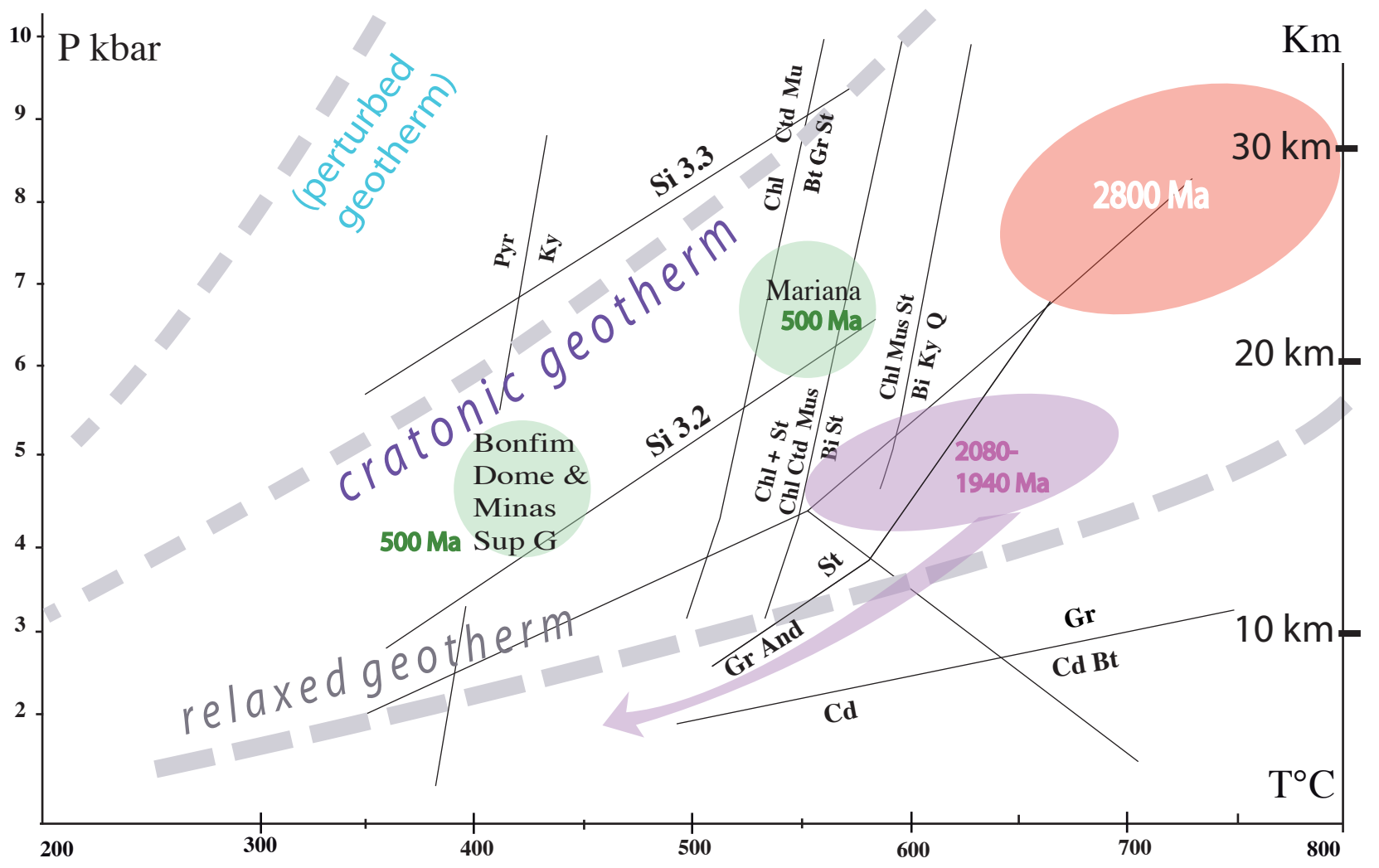
P kbar
Km
10
9
8
7
6
5
4
3
2
200
300
400
500
600
700
800
T°C
30 km
20 km
10 km
(perturbed geotherm)
cratonic geotherm
relaxed geotherm
Si 3.3
Si 3.2
Pyr
Ky
Chl
Ctd Mu
Bt Gr St
Chl Mus St
Bi Ky Q
Chl + St
Chl Ctd Mus
Bi St
St
Gr And
Gr
Cd Bt
Cd
Mariana
500 Ma
Bonfim
Dome &
Minas
500 Ma Sup G
2800 Ma
2080-
1940 Ma

Figure 9

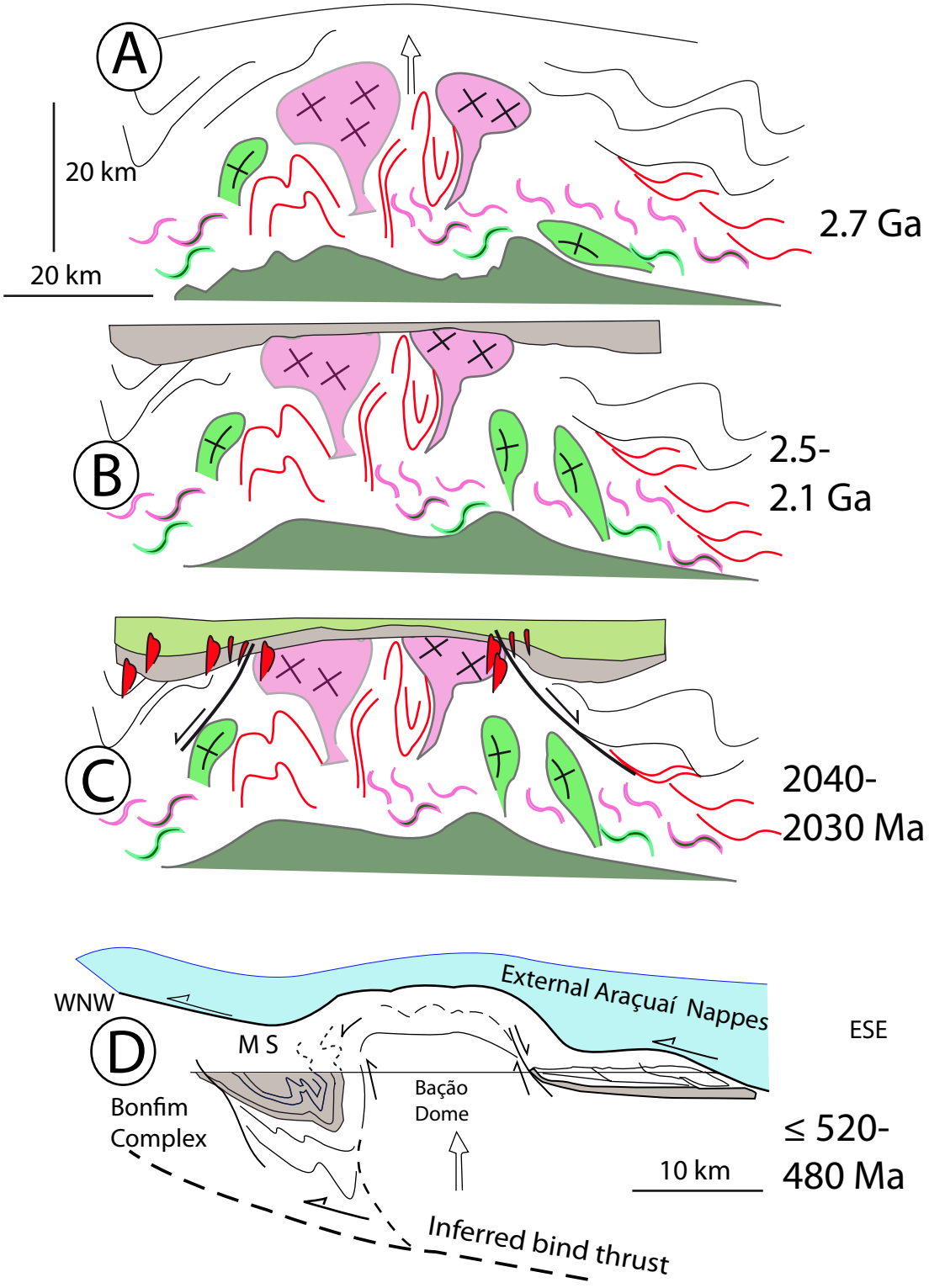
A
20 km
20 km
2.7 Ga
B
2.5-
2.1 Ga
C
2040-
2030 Ma
WNW
D
M S
External Araçuaí Nappes
ESE
Bação
Dome
Bonfim
Complex
10 km
≤ 520-
480 Ma
Inferred bind thrust
1
2
3
4
5
a
b
6
7

Figure 10